**Interaction of tetraspan(in) TM4SF5 with CD44 promotes self-renewal and circulating capacities of hepatocarcinoma cells**

Doohyung Lee[1], Juri Na[2,*], Jihye Ryu[1,*], Hye-Jin Kim[1,*], Seo Hee Nam[3,*], Minkyung Kang[1,4], Jae Woo Jung[3], Mi-Sook Lee[1], Haeng Eun Song[1], Jungeun Choi[3], Gyu-Ho Lee[1], Tai Young Kim[1], June-Key Chung[2,5], Ki Hun Park[6], Sung-Hak Kim[7], Hyunggee Kim[7], Howon Seo[8], Pilhan Kim[8], Hyewon Youn[2,5], and Jung Weon Lee[1,3,9]

[1]Department of Pharmacy, College of Pharmacy, Research Institute of Pharmaceutical Sciences, Seoul National University, [2]Department of Nuclear Medicine, Cancer Research Institute, College of Medicine, Seoul National University, [3]Interdisciplinary Program in Genetic Engineering, Seoul National University, [4]Department of Biomedical Sciences, College of Medicine, Seoul National University, Seoul 110-799, [5]Cancer Imaging Center, Seoul National University Hospital, Seoul 110-799, [6]Division of Applied Life Science, Gyeongsang National University, Jinju 660-701, [7]School of Life Sciences and Biotechnology, Korea University, Seoul 136-713, Korea (Republic of), [8]Graduate School of Nanoscience and Technology, Korea Advanced Institute of Science and Technology, Daejeon 305-701, Korea (Republic of). *; equally contributed.

[9]Contact information: Jung Weon Lee, Ph.D. Department of Pharmacy, College of Pharmacy, Seoul National University, Seoul 1510742, Korea [jwl@snu.ac.kr, +8228802495 (☎), +8228721795 (Fax)].

**Running title:** TM4SF5-mediated self-renewal property

**Key words**: biomarkers; circulating tumor cells; epithelial-mesenchymal transition; hepatic cancer; self-renewal.

**Financial Supports**

This work was supported by a grant of the Korea Health Technology R&D Project through the KHIDI, Republic of Korea (HI14C1072 to HY), and by the NRF of Korea grant for the Tumor Microenvironment GCRC funded by the Korea (Ministry of Science, ICT & Future Planning) (2011-0030001 to HY and JWL), for senior Leap research (2012-0005606/2013-035235), and for Medicinal Bioconvergence Research Center (NRF-2012M3A6A4054271) to JWL.

## Abstract

Tumor metastasis involves circulating and tumor-initiating capacities of metastatic cancer cells. Epithelial-mesenchymal transition is related to self-renewal capacity and circulating tumor cell (CTC) characteristics for tumor metastasis. Although tumor metastasis as a life-threatening complicated process occurs through circulation of tumor cells, mechanistic aspects of self-renewal and circulating capacities have been largely unknown. Hepatic TM4SF5 promotes EMT for malignant growth and migration, so that it was rationalized TM4SF5 as a hepatocellular carcinoma (HCC) biomarker might be important for metastatic potentials throughout metastasis. Here, self-renewal capacity by TM4SF5 was mechanistically explored using hepatocarcinoma cells with or without TM4SF5 expression, and explored whether they became CTCs using mouse liver-orthotopic model systems. We found that TM4SF5-dependent sphere growth correlated with $CD24^-$, ALDH activity, and a physical association between CD44 and TM4SF5. The interaction between TM4SF5 and CD44 was through their extracellular domains with *N*-glycosylation modifications. The TM4SF5/CD44 interaction activated c-Src/STAT3/Twist1/Bmi1 signaling for spheroid formation, while disturbing the interaction, expression, or activity of any component in this signaling pathway inhibited the spheroid formation. In serial xenografts using 200 ~ 5000 cells per injection, TM4SF5-positive tumors exhibited subpopulations with locally-increased CD44 expressions, supporting for tumor cell differentiation. TM4SF5-positive, but not

TM4SF5- or CD44-knocked-down, cells were identified circulating in blood 4 to 6 weeks after orthotopic liver-injection using an *in vivo* laser scanning endomicroscopy. Anti-TM4SF5 reagent blocked their metastasis to distal intestinal organs. ***Conclusion*:** Altogether, our results evidence that TM4SF5 promotes self-renewal and CTC properties supported by $TM4SF5^{+}/CD44^{+(TM4SF5\text{-}bound)}/ALDH^{+}/CD24^{-}$ markers, during HCC metastasis.

## INTRODUCTION

Hepatocellular carcinoma (HCC) is the third most common cause of mortality due to cancer.[1] Although hepatic resection and liver transplantation represent first–line treatments for HCC,[2] the second-line treatment for HCC patient in advanced stages has shown limited efficacy.[3] Moreover, the metastatic recurrence renders this carcinoma resistant to any significant chemopreventive effects.

Epithelial-mesenchymal transition (EMT), the process by which epithelial cells lose their polarity and gain mesenchymal traits,[4] was shown to generate stem cells in mammary epithelial models.[5] EMT has been suggested to play roles in formation of circulating tumor cells (CTCs), which can eventually form metastatic tumors.[6] Metastatic cells that have undergone EMT are thought to resemble cancer stem cells (CSCs),[7] because they can initiate tumor growth after colonization at a distant region, and are enriched for genes associated with stemness as well as drug resistance.[8] Although previous reports suggested that CSCs may arise from transformation of normal cells, more recent reports have suggested that these cells are derived from fully differentiated cells through adaptive trans-differentiation mechanisms, such as EMT.[5] Therefore, CTCs may acquire self-renewal capacity during cancer metastasis.[9] However, the molecules responsible for the acquisitions of these CTCs characteristics are not fully known.

As a tetraspan(in), TM4SF5 is highly expressed in diverse cancers such as HCC, induces

EMT, and collaborates with integrins,[10] resulting in morphological elongation through actin reorganization.[11] Moreover, gefitinib resistance in non-small cell lung cancer depends on TM4SF5-mediated EMT.[12]

Because TM4SF5 induces EMT, we hypothesized that TM4SF5 may be involved in generating CTC phenotypes in HCC. Here using *in vitro* cells and an *in vivo* animal system, we observed an interaction between TM4SF5 and CD44 that conferred self-renewal properties via the signaling pathway involving c-Src, STAT3, Twist1, and Bmi1, leading to the presence of TM4SF5-dependent metastatic CTCs in the blood.

## Experimental Procedures

***Cells.*** HCC cells, including SNU449 cells expressing WT TM4SF5 (SNU449Tp pooled clone, $T_3$, $T_7$, $T_{10}$, and $T_{16}$ single cell-derived clones), *N*-glycosylation mutants of TM4SF5 [N138A, N155Q, or N138A/N155Q (NANQ)], or no TM4SF5 [SNU449 parental (P) or the Cp negative pooled clone], were previously described.[11] Huh7 cells endogenously or SNU449$T_7$ clone exogenously expressing TM4SF5 were stably transfected with a scrambled control shRNA (tGFP-shScram in pGFP-V-RS plasmid, OriGene, Rockville, MD) or shRNA against TM4SF5.[13] [tGFP-shTM4SF5 in pGFP-V-RS plasmid, Cat. #: TG308787, OriGene). SNU449 and SNU761 cells did not express detectable levels of TM4SF5, whereas Huh7 and HepG2 cells express TM4SF5.[14] SNU449$T_7$ cells were also stably transfected with shRNA against CD44 (Addgene, Cambridge, MA). Cells were maintained in RPMI-1640 medium (WelGene, Daegu, Korea) containing 10% FBS and 1% penicillin/streptomycin (GenDEPOT Inc. Barker, TX).

***Spheroid Formation Assay.*** Cells were collected, washed twice with PBS to remove serum, and then suspended in serum-free DMEM/F12 media supplemented with 1% penicillin/streptomycin (GenDEPOT Inc.) and 2% B27 supplement (Invitrogen, Grand Island, NY). Human EGF and bFGF (25 ng/ml, PeproTech, Rocky Hill, NJ) were added to the culture every other day. The cells were subsequently cultured in ultra-low attachment 6-well plates (Corning Inc., Corning, NY) at a density of no more than $5 \times 10^3$ cells/well with or

without specific inhibitors against TM4SF5 [20 μM TSAHC[15]], c-Src (20 μM PP2, LC Labs, Woburn, MA), or STAT3 (1 ~ 4 μM STATtics). The representative spheroid images were photographed using a microscope (CKX41, Olympus, Tokyo, Japan) or a time-lapse IX81-ZDC microscope (Olympus).

***Western Blots.*** Spheroids or subconfluent cells in media containing 10% FBS were harvested as whole cell lysates using a modified RIPA lysis buffer containing 0.1% SDS, 0.5% deoxycholate, 1% NP-40, and proteinase inhibitors.[11] Tissue extracts from human or mouse livers were also prepared as previously described.[11]

***Flow Cytometry.*** Stable SNU449 cell clones with or without TSAHC treatment, cells prepared from primary or secondary xenograft tumors, and cells sorted from blood samples were processed for FACS analysis, as previously described.[16]

***Analyses of Mouse or Human Tissues.*** All procedures using animal and human tissues were performed in accordance with the procedures of the Seoul National University Institutional Review Board (SNUIRB) agreement.

***Statistical Methods.*** Student's *t*-tests were performed for statistical comparisons of mean values. A *p* value less than 0.05 was considered statistically significance.

**Supplementary Information**

Supplementary figures and information on *cell culture, drug sensitivity, RT-PCR, western blots, coimmunoprecipitations*, *ALDERFLUOR assay, flow cytometry, serial mouse*

*xenografts, immunohistochemistry of mouse or human tissues, and orthotopic tumor cell injection and blood collection for CTC identification can be found at the journal web site.*

## Results

Ectopic TM4SF5 expression in SNU449 HCC cells was associated with loss of cell-cell adhesion molecule expression, and concomitant induction of mesenchymal markers (Fig. S1A). Furthermore, knockdown of endogenous TM4SF5 in Huh7 cells increased the expression of cell-cell adhesion molecules but decreased mesenchymal markers (Fig. S1B). Moreover, TM4SF5 expression correlated with the resistance of cells to the anti-cancer agent paclitaxel (Fig. S1C). Because EMT and drug resistance characteristics were associated with TM4SF5, TM4SF5-mediated self-renewal properties were further explored.

### *TM4SF5 Expression Promoted Spheroid Formation in HCC*

We first tested whether TM4SF5 could form spheroids in a low-adhesive environment. Unlike the TM4SF5-null SNU449 and SNU761 HCC cell lines, Huh7 and HepG2 HCC cells with endogenous TN4SF5[14] formed spheroids (Fig. 1A). TM4SF5-expressing SNU449 transfectants (SNU449Tp, pooled clone; $T_3$, $T_7$, $T_{10}$, and $T_{16}$, single cell-derived clones) readily formed spheroids, whereas the TM4SF5-negative pooled clone (SNU449Cp) and the *N*-glycosylation mutants (N138A, N115Q, or N138A/N155Q) cells did not (Fig. 1B). The number of spheroids larger than 70 μm correlated with wild type (WT) TM4SF5 expression (Fig. 1C). Aldehyde dehydrogenase enzyme activities were higher in WT TM4SF5 expressing cells than in TM4SF5-null or mutant-expressing cells (Figs. 1D, S1D). TM4SF5-knockdown in Huh7 cells exhibited decreased phospho-FAK, $p27^{Kip1}$ expression, and

phospho-Ser10 $p27^{Kip1}$ levels (Fig. 1E), as expected based on a previous study,[11] and formed fewer spheroids (Fig. 1F). TM4SF5 knockdown in stable $SNU449T_7$ cells also abolished spheroid formation (Fig. S2). Taken together, the results demonstrated that TM4SF5 was thus involved in spheroid formation.

***TM4SF5 Interacted with CD44 for Spheroid Formation***

We next examined the expression levels of molecules that might be associated with self-renewal. *CD24* mRNA expression was lower in TM4SF5-postive cells than in TM4SF5-negative cells, whereas *CD44* mRNA expression was similar in both TM4SF5-negative and -positive cells (Fig. 2A). The protein levels showed similar patterns by western blots and FACS analysis (Figs. 2B, 2C, and 2D). The anti-CD44 clone IM7 (BioLegend, San Diego, CA) revealed similar CD44 expression levels on TM4SF5-negative or mutant cells and WT TM4SF5-expressing cells (Fig. 2D, upper), whereas the anti-CD44 clone DF1485 (Santa Cruz Biotechnology, Santa Cruz, CA) showed a positive signal only in TM4SF5-negative or mutant cells (Fig. 2D, lower). This difference may have been due to differential epitope availability in CD44, which presumably resulted from a different conformational context due to TM4SF5 expression and/or interaction. Treatment with the anti-TM4SF5 reagent, TSAHC, which disrupts the *N*-glycosylation pattern of TM4SF5,[15] did not change CD44 levels on TM4SF5-negative or mutant cells, but slightly increased CD44 levels on WT TM4SF5 expressing cells (Fig. 2E), although TSAHC did not cause additional *CD44* mRNA

transcription (Fig. 2F). Furthermore, the WT TM4SF5, but not the *N*-glycosylation mutant, did not co-immunoprecipitate with endogenous CD44 (Fig. 3A). This TM4SF5-CD44 interaction occurred through extracellular domains; the CD44-$\Delta_{ICD}$ (deletion mutant without the intracellular domain) was pulled-down by STrEP-tagged WT TM4SF5 (Fig. 3B), again depending on TSAHC treatment (Fig. 3C). Knockdown of TM4SF5 also increased the level of CD44 recognized by anti-CD44 DF1485 antibody (Fig. 3D). Consistently, WT TM4SF5-dependent spheroid formation was abolished by TSAHC treatment (Fig. 3E), and by CD44 knockdown (Fig. 3F). Therefore, the physical association between CD44 and TM4SF5 appeared critical for TM4SF5-mediated spheroid formation.

***Self-renewal Properties Were Controlled by TM4SF5 Expression***

When fewer than 5,000 SNU449Cp (or $TM4SF5_{N138A/N155Q}$) or WT TM4SF5-positive $SNU449T_7$ cells were subcutaneously injected into the left or right flanks of mice, $SNU449T_7$ cells clearly formed tumors, while the control or mutant cells did not (Fig. 4A). Cells purified from the primary xenografts (i.e., $ExpT_7$ cells of mouse #2, $ExpT_{7\text{-}2}$) showed similar or greater TM4SF5 expression and TM4SF5-downstream signaling activities, compared with those in original $SNU449T_7$ cells (Fig. 4A, middle immunoblot panel). $ExpT_{7\text{-}2}$ cells formed more aggressive spheroids than $SNU449T_7$ cells (Fig. 4A, bottom spheroid image). $ExpT_{7\text{-}2}$ or $ExpT_{7\text{-}3}$ cells formed tumors more aggressively and at cell numbers as low as 200 cells/injection in secondary xenografts (Figs. 4B, S3A). Consistently, the cells purified from

the secondary xenografts (i.e., $^{2nd}ExpT_{7-2}$) exhibited a further increase in phospho-c-Src levels, compared with the SNU449Cp, $SNU449T_7$, or $ExpT_{7-2}$ cells (Fig. 4B, bottom).

Using WT TM4SF5-dependent xenografts tissues, double-immunohistochemistry for TM4SF5 and CD44 showed distinct cell populations with either higher CD44 level (reddish) or both TM4SF5 and CD44 (yellowish) expression levels (Fig. 4C). $SNU449T_7$ cells could have thus differentiated into heterogeneous cell types with varied TM4SF5 and/or CD44 expression levels during xenograft formation. When analyzed by FACS, CD44 (as measured by the IM7 antibody clone) and TM4SF5 were more highly expressed in $ExpT_{7-2}$, $ExpT_{7-3}$, and $^{2nd}ExpT_{7-2}$ cells compared to the original $SNU449T_7$ cells (Figs. 4D, S3B). However, the surface levels of CD24, CD90, and CD133 were unchanged, suggesting that these markers might not be involved in TM4SF5-mediated effects. Dual labelling of $ExpT_{7-2}$ or $ExpT_{7-3}$ produced histograms showing populations with either increased expression of CD44 or TM4SF5, or an increase in both markers (Fig. 4E).

***TM4SF5 Regulates c-Src, STAT3, Twist1, and Bmi1 for Self-renewal Properties***

Phospho-Tyr416 c-Src, phospho-Tyr705 STAT3, *Twist1* mRNA, and *Bmi1* mRNA levels correlated with TM4SF5-mediated spheroid formation (Fig. 5A). Knockdown of either TM4SF5 or CD44 in $SNU449T_7$ cells reduced their levels, and negatively affected the phosphorylation of FAK and $p27^{Kip1}$ downstream of TM4SF5.[11] However, CD44 knockdown did not reduce phospho-Ser10 $p27^{Kip1}$ (Figs. 5B, C). Furthermore, the xenografts formed from

SNU449$T_7$ cells (mice #2 and #3) exhibited co-expression of CD44 and Bmi1 within TM4SF5-positive areas (Fig. 5D).

Treatment of TM4SF5-expressing cell clones with TSAHC decreased the levels of phosho-Tyr416 c-Src, phospho-Tyr705 STAT3, Twist1, and *Bmi1* mRNA (Fig. 5E). As TSAHC treatment of Huh7 cells abolished spheroid formation (Fig. 5F, top), TSAHC decreased the TM4SF5-mediated signaling levels and *Bmi1* mRNA levels, compared with DMSO treatment (Fig. 5F, bottom). Treatment of WT TM4SF5-expressing SNU449$T_7$ cells with PP2 (but not the control PP3) blocked TM4SF5-dependent spheroid formation (Fig. 6A). Treatment of SNU449$T_7$ cells with a STST3 inhibitor (STATtic) abolished spheroid formation (Fig. 6B). After c-Src or STAT3 inhibition, phospho-Tyr705 STAT3 and Twist1 expression decreased, although caspase 3 activation was not observed (Fig. S4), suggesting that c-Src acted upstream of STAT3, which again acted upstream of Twist1.

Overexpression of Bmi1 into TM4SF5-null or -mutant (NANQ) cell clones was sufficient to promote spheroid-formation (Fig. 6C). Meanwhile, knockdown of Bmi1 in SNU449$T_7$ cells blocked spheroid formation (Fig. 6D). TM4SF5 thus required Bmi1 expression for spheroid formation. Immunostaining of HCC tumor tissue revealed colocalization of TM4SF5 and Bmi1 with local CD44 expression (Fig. 6E), similar to the results obtained for mouse xenografts (Figs. 4C, 5D). In addition, the Oncomine$^{TM}$ database revealed that TM4SF5 expression in liver cancer tissues significantly correlates with Bmi1 expression (Fig.

S5).

***Identification of TM4SF5-Dependent CTCs and Their Metastasis***

SNU449T$_7$ cells stably transfected with tGFP-tagged shRNA constructs against a scrambled sequence (tGFP-shScram) or TM4SF5 (tGFP-shTM4SF5) or the PBS vehicle alone were injected orthotopically into mouse livers. Four or six weeks later, blood samples were collected and assayed by anti-tGFP and DAPI staining. No cells were found in the blood samples of mice injected with PBS or SNU449T$_7$-(tGFP)-shTM4SF5 cells, whereas TM4SF5-positive cells were found in mice injected with SNU449T$_7$-(tGFP)-shScram cells (Figs. 7A, B). The tGFP signal was also examined in live mice using confocal laser endomicroscopy. When 0.453 mm$^3$ sections of blood vessels were analyzed for 20 min, two out of three SNU449T$_7$-(tGFP)-shScram mice exhibited streaming tGFP-positive cells (Fig. 7C), whereas none of the SNU449T$_7$-(tGFP)-shTM4SF5 mice showed positive cells (data not shown). After endomicroscopic imaging, blood samples from mice injected with SNU449T$_7$-(tGFP)-shScram cells contained green-fluorescent cells (Fig. S6). Furthermore, SNU449T$_7$-shControl cells that were orthotopically injected into livers were recovered as DAPI-positive cells in blood samples, whereas no such positive cells were observed in blood from mice injected with PBS or SNU449T$_7$.shCD44 cells (Fig. 7D). SNU449T$_7$-shScramble cell-injected mice exhibited shorter life spans, while PBS-injected or SNU449T$_7$.shCD44 cell-injected mice survived (Fig. 7D).

Orthotopic liver-injection of SNU449$T_7$-shControl cells after incision was followed by treatment with either DMSO or TSAHC. Whereas DMSO-treated mice showed metastatic cell settlements distal from cell-injected livers (8/8 mice, 100%) after a 2 week-treatment, TSAHC treatment obviously inhibited metastatic cell populations (3/8 mice, 37.5%) (Fig. 8A). Total signal flux from the injected and metastatic cell populations were significantly reduced after 3 week of TSAHC treatment (Fig. 8B). We further evaluated the metastasis after abdominal surgery (Fig. 8C). Quantitation after abdominal surgery showed a lower level of total flux in TSAHC-treated animals ($p$ = 0.18, n = 8) and a significantly-lower ($p$ = 0.0287, n = 8) number of the metastatic cell populations in TSAHC-treated animals, compared with DMSO-treated control mice (Fig. 8D). The metastatic populations were related mostly with the intestinal area and blocked by TSAHC treatments (Fig. 8E).

## DISCUSSION

This study revealed that TM4SF5 bound CD44, and the interaction regulated the levels or activities of c-Src/STAT3/Twist1/Bmi1 to control the self-renewal properties of HCCs, subsequently promoting the CTC capacity for metastasis (Fig. 8F). Furthermore, TM4SF5-dependent self-renewal and CTC properties were characterized by the molecular status of $TM4SF5^{+}/CD24^{-}/CD44^{(TM4SF5\text{-}bound)}$/ALDH, leading to the c-Src/STAT3/Twist1/Bmi1 pathway. Knockdown or inhibition of any of these molecules inhibited the self-renewal capacity. While TM4SF5-expressing cells orthotopically injected into mouse livers were observed in the blood and intestine of mice, knockdown of TM4SF5 or CD44, or inhibition of their interaction, abolished the detection of CTCs in the blood stream and their colonization to distal organs like the intestine.

TM4SF5 is expressed in fibrotic livers following $CCl_4$ administration and its antagonist blocks the chemically-mediated liver fibrosis.[17] Mice administered chronic ethyl alcohol feeding for 4 weeks increased TM4SF5 expression in livers and TM4SF5 transgenic mice showed fatty livers 12 month after birth (unpublished data). TGFβ1 or the conditioned media containing EGF from activated hepatic stellate cells causes Smad4 activation that leads to EGFR/ERKs signaling for TM4SF5 expression.[18] TGFβ1, phospho-Smads, α-smooth muscle actin, collagen I, and TM4SF5 are co-stained along the fibrotic septa that run between the areas of the centrilobular bridging fibrosis in the fibrotic livers, but not in control livers.[17]

Furthermore, TM4SF5 is highly expressed in liver cancer tissues, compared with normal liver tissues[11]. Therefore, TM4SF5 appears to be expressed in pathological livers following chronic-injuries, leading to gradual development of malignant fibrosis and tumorigenesis.

TM4SF5-dependent self-renewal properties could be related to TM4SF5-mediated EMT[11] and drug resistance.[12] The self-renewal property of metastatic cancer cells is important for tumor expansion after colonization at distal sites. Assuming that CTCs may be clinically important targets for drug development, the ability of TM4SF5 to mediate EMT, self-renewal, and CTC properties makes it a promising drug target. TM4SF5 may localize to tetraspan(in)-enriched microdomains (TEMs), where it can form massive protein complexes with integrins and growth factor receptors.[10] Protein complexes at TEMs may transduce signals that regulate diverse cellular functions.[19] In this current study, we showed that TM4SF5 interacted with CD44 through its extracellular domain, depending on the *N*-glycosylation status of TM4SF5. CD44 has been identified as a lymphocyte homing receptor[20] and also a proteoglycan that is also commonly expressed in epithelial and cancer cells.[21] CD44 is overexpressed in HCC for a poor prognosis,[22,23] and immunohistochemistry of a limited number of clinical samples in our current study showed a regionally-increased CD44 expression in liver cancer tissues, compared with matched-pair normal liver tissues. Diverse HCC cell lines differentially expressed CD44.[24] Although CD44 expression is also required for the maintenance of stem cell phenotypes in breast cancer cells,[25] it has been

suggested that CD44 can be more useful when combined with other markers to support for the stemness in HCC.[26] Furthermore, the isoform conversion between standard CD44 (CD44s) and variant CD44 (CD44v) may be important for tumor initiation and maintenance.[27] Indeed, we found that hepatic epithelial cells in our current study showed a comparable CD44 expression independent of TM4SF5 expression, and the open database of Oncomine also showed no significant difference in CD44 expression between normal and cancer liver samples, while TM4SF5 and Bmi1 were highly enhanced in cancer liver samples (Fig. S6). Although the relationship between TM4SF5 and CD44 protein levels in more clinical HCC tissues should be confirmed in next studies, it is likely that interaction between CD44 and TM4SF5 resulted in tumor initiating and circulating properties via interaction-mediated signaling and the EMT phenotype.

TM4SF5 was previously shown to promote FAK[28] and c-Src activation,[13] and expression of the TM4SF5 *N*-glycosylation mutant or treatment with TSAHC abolished TM4SF5-mediated FAK/c-Src signaling and EMT.[11] Moreover, knockdown of either TM4SF5 or CD44 in SNU449T$_7$ cells decreased both c-Src and STAT3 phosphorylations, thereby inhibiting sphere growth. In the present study, c-Src acted upstream of STAT3 phosphorylation, as shown in a previous study.[29] STAT3 is activated in 50% of HCC,[30] where STAT3 Tyr705 is phosphorylated in an IL6-independent manner.[31] STAT3 signaling in HCCs can not only regulate genes involved in cell growth, survival, immune suppression, and angiogenesis but

also promote metastasis.[32] Highly-activated STAT3 in HCCs binds to the promoter of the *Twist1* gene to increase *Twist1* mRNA expression.[33] Bmi1 is directly upregulated by Twist1 and essential for Twist1-induced EMT,[34] and Bmi1 is also associated with stemness, leading to cancer recurrence and chemoresistance.[35] Moreover, Bmi1, which is upregulated in many cancer types, is highly expressed in $CD133^+$ murine liver CSCs,[36] and enriched in CSCs with other stemness markers including CD44,[37] being consistent with this current study. TM4SF5-mediated spheroid formation may not need CD90 or CD133, as their expressions were not depending on TM4SF5, although CD133 appears to act upstream of TM4SF5 (unpublished observations). Being consistent, CD133 and CD44 are considered markers for cancer stem cells in HCC.[38,39]

TSAHC has been shown not to cause any cytostatic effects in normal TM4SF5-negative hepatocytes.[15,40] Intraperitoneal TSAHC treatment given alone to mice (50 $mg/kg^{-1}$) in 40% dimethylsulfoxide or orally (250 $mg/kg^{-1}$) in 5% carboxymethylcellulose for 4 weeks shows the anatomical appearance of livers comparable to control livers, and does not cause any mortality, although the TSAHC treatment together with $CCl_4$ administration decreases $CCl_4$-mediated fibrotic phenotypes.[17] In the present study, TM4SF5-positive cells orthotopically-injected into mice livers efficiently metastasized to the intestine and peritoneal membrane, in addition to tail vein-injected cells,[41] which were inhibited by the anti-TM4SF5 reagent TSAHC. TM4SF5-mediated metastasis might have occurred via TM4SF5-dependent CTC

properties supported by the TM4SF5/CD44/c-Src/STAT3/Twist1/Bmi1 pathway. Thus, it is likely that TM4SF5-positive cancer cells can circulate throughout the blood and lymph nodes for eventual metastasis, and targeting TM4SF5 or the interaction between TM4SF5 and CD44 may lead to efficient inhibition of TM4SF5-mediated metastasis.

## AUTHOR CONTRIBUTIONS

DL performed most experiments. JR, HES, and MK help with human tissue IHC. HJK, JC, GHL, and TYK helped with coimmunoprecipitations and constructs. SHN and MSL helped with spheroid imaging. JWJ and PK, JN, and HY helped with animal imaging. SHK and HK helped with spheroid cultures. JWL planed the experiments, interpreted the data, and wrote manuscript.

## COMPETING FINANCIAL INTERESTS

The authors declare no competing financial interests.

**REFERENCES**


1. Parkin DM, Bray F, Ferlay J, Pisani P. Global cancer statistics, 2002. CA Cancer J Clin 2005;55:74-108.
2. Kassahun WT, Fangmann J, Harms J, Hauss J, Bartels M. Liver resection and transplantation in the management of hepatocellular carcinoma: a review. Exp Clin Transplant 2006;4:549-558.
3. Kuvshinoff BW, Ota DM. Radiofrequency ablation of liver tumors: influence of technique and tumor size. Surgery 2002;132:605-611.
4. Lee JM, Dedhar S, Kalluri R, Thompson EW. The epithelial-mesenchymal transition: new insights in signaling, development, and disease. J Cell Biol 2006;172:973-981.
5. Mani SA, Guo W, Liao MJ, Eaton EN, Ayyanan A, Zhou AY, Brooks M, et al. The epithelial-mesenchymal transition generates cells with properties of stem cells. Cell 2008;133:704-715.
6. Thiery JP, Lim CT. Tumor Dissemination: An EMT Affair. Cancer Cell 2013;23:272-273.
7. Brabletz T, Jung A, Spaderna S, Hlubek F, Kirchner T. Opinion: migrating cancer stem cells - an integrated concept of malignant tumour progression. Nat Rev Cancer 2005;5:744-749.
8. Dean M, Fojo T, Bates S. Tumour stem cells and drug resistance. Nat Rev Cancer 2005;5:275-284.
9. Tiwari N, Gheldof A, Tatari M, Christofori G. EMT as the ultimate survival mechanism of cancer cells. Semin Cancer Biol 2012;22:194-207.
10. Lee SA, Park KH, Lee JW. Modulation of signaling between TM4SF5 and integrins in tumor microenvironment. Front Biosci 2011;16:1752-1758.
11. Lee SA, Lee SY, Cho IH, Oh MA, Kang ES, Kim YB, Seo WD, et al. Tetraspanin TM4SF5 mediates loss of contact inhibition through epithelial-mesenchymal transition in human hepatocarcinoma. J Clin Invest 2008;118:1354-1366.
12. Lee MS, Kim HP, Kim TY, Lee JW. Gefitinib resistance of cancer cells correlated with TM4SF5-mediated epithelial-mesenchymal transition. Biochim Biophys Acta 2012;1823:514-523.
13. Jung O, Choi YJ, Kwak TK, Kang M, Lee MS, Ryu J, Kim HJ, et al. The COOH-terminus of TM4SF5 in hepatoma cell lines regulates c-Src to form invasive protrusions via EGFR Tyr845 phosphorylation. Biochim Biophys Acta 2013;1833:629-642.
14. Choi S, Oh SR, Lee SA, Lee SY, Ahn K, Lee HK, Lee JW. Regulation of TM4SF5-mediated tumorigenesis through induction of cell detachment and death by tiarellic acid. Biochim Biophys Acta 2008;1783:1632-1641.
15. Lee SA, Ryu HW, Kim YM, Choi S, Lee MJ, Kwak TK, Kim HJ, et al. Blockade of four-

transmembrane L6 family member 5 (TM4SF5)-mediated tumorigenicity in hepatocytes by a synthetic chalcone derivative. Hepatology 2009;49:1316-1325.

16. Kim H-P, Kim T-Y, Lee M-S, Jong H-S, Kim T-Y, Weon Lee J, Bang Y-J. TGF-[beta]1-mediated activations of c-Src and Rac1 modulate levels of cyclins and p27Kip1 CDK inhibitor in hepatoma cells replated on fibronectin. Biochimica Biophysica Acta 2005;1743:151-161.
17. Kang M, Jeong SJ, Park SY, Lee HJ, Kim HJ, Park KH, Ye SK, et al. Antagonistic regulation of transmembrane 4 L6 family member 5 attenuates fibrotic phenotypes in CCl(4) -treated mice. FEBS J 2012;279:625-635.
18. Kang M, Choi S, Jeong SJ, Lee SA, Kwak TK, Kim H, Jung O, et al. Cross-talk between TGFβ1 and EGFR signalling pathways induces TM4SF5 expression and epithelial-mesenchymal transition. Biochem J 2012;443:691-700.
19. Hemler ME. Tetraspanin proteins mediate cellular penetration, invasion, and fusion events and define a novel type of membrane microdomain. Annu Rev Cell Dev Biol 2003;19:397-422.
20. Gallatin WM, Weissman IL, Butcher EC. A cell-surface molecule involved in organ-specific homing of lymphocytes. Nature 1983;304:30-34.
21. Williams K, Motiani K, Giridhar PV, Kasper S. CD44 integrates signaling in normal stem cell, cancer stem cell and (pre)metastatic niches. Exp Biol Med (Maywood) 2013;238:324-338.
22. Endo K, Terada T. Protein expression of CD44 (standard and variant isoforms) in hepatocellular carcinoma: relationships with tumor grade, clinicopathologic parameters, p53 expression, and patient survival. J Hepatol 2000;32:78-84.
23. Mima K, Okabe H, Ishimoto T, Hayashi H, Nakagawa S, Kuroki H, Watanabe M, et al. CD44s regulates the TGF-β-mediated mesenchymal phenotype and is associated with poor prognosis in patients with hepatocellular carcinoma. Cancer Res 2012;72:3414-3423.
24. Okabe H, Ishimoto T, Mima K, Nakagawa S, Hayashi H, Kuroki H, Imai K, et al. CD44s signals the acquisition of the mesenchymal phenotype required for anchorage-independent cell survival in hepatocellular carcinoma. Br J Cancer 2014;110:958-966.
25. Pham PV, Phan NL, Nguyen NT, Truong NH, Duong TT, Le DV, Truong KD, et al. Differentiation of breast cancer stem cells by knockdown of CD44: promising differentiation therapy. J Transl Med 2011;9:209.
26. Liu LL, Fu D, Ma Y, Shen XZ. The power and the promise of liver cancer stem cell markers. Stem Cells Dev 2011;20:2023-2030.
27. Prochazka L, Tesarik R, Turanek J. Regulation of alternative splicing of CD44 in cancer. Cell Signal 2014;26:2234-2239.

28. Jung O, Choi S, Jang SB, Lee SA, Lim ST, Choi YJ, Kim HJ, et al. Tetraspan TM4SF5-dependent direct activation of FAK and metastatic potential of hepatocarcinoma cells. J Cell Sci 2012;125:5960-5973.
29. Schaefer LK, Wang S, Schaefer TS. c-Src activates the DNA binding and transcriptional activity of Stat3 molecules: serine 727 is not required for transcriptional activation under certain circumstances. Biochem Biophys Res Commun 1999;266:481-487.
30. Subramaniam A, Shanmugam MK, Perumal E, Li F, Nachiyappan A, Dai X, Swamy SN, et al. Potential role of signal transducer and activator of transcription (STAT)3 signaling pathway in inflammation, survival, proliferation and invasion of hepatocellular carcinoma. Biochim Biophys Acta 2013;1835:46-60.
31. Ryu J, Kang M, Lee MS, Kim HJ, Nam SH, Song HE, Lee D, et al. Cross-talk between the TM4SF5/FAK and the IL6/STAT3 pathways renders immune escape of human liver cancer cells. Mol Cell Biol 2014;34:2946-2960.
32. Li WC, Ye SL, Sun RX, Liu YK, Tang ZY, Kim Y, Karras JG, et al. Inhibition of growth and metastasis of human hepatocellular carcinoma by antisense oligonucleotide targeting signal transducer and activator of transcription 3. Clin Cancer Res 2006;12:7140-7148.
33. Cheng GZ, Zhang WZ, Sun M, Wang Q, Coppola D, Mansour M, Xu LM, et al. Twist is transcriptionally induced by activation of STAT3 and mediates STAT3 oncogenic function. J Biol Chem 2008;283:14665-14673.
34. Yang MH, Hsu DS, Wang HW, Wang HJ, Lan HY, Yang WH, Huang CH, et al. Bmi1 is essential in Twist1-induced epithelial-mesenchymal transition. Nat Cell Biol 2010;12:982-992.
35. Cao L, Bombard J, Cintron K, Sheedy J, Weetall ML, Davis TW. BMI1 as a novel target for drug discovery in cancer. J Cell Biochem 2011;112:2729-2741.
36. Oishi N, Wang XW. Novel therapeutic strategies for targeting liver cancer stem cells. Int J Biol Sci 2011;7:517-535.
37. Siddique HR, Saleem M. Role of BMI1, a stem cell factor, in cancer recurrence and chemoresistance: preclinical and clinical evidences. Stem Cells 2012;30:372-378.
38. Zhu Z, Hao X, Yan M, Yao M, Ge C, Gu J, Li J. Cancer stem/progenitor cells are highly enriched in CD133+CD44+ population in hepatocellular carcinoma. Int J Cancer 2010;126:2067-2078.
39. Poon RWCPaRTP. Cancer Stem Cell as a Potential Therapeutic Target in Hepatocellular Carcinoma. Current Cancer Drug Targets 2012;12:1081-1094.
40. Lee SA, Lee MS, Ryu HW, Kwak TK, Kim H, Kang M, Jung O, et al. Differential inhibition of transmembrane 4 L six family member 5 (TM4SF5)-mediated tumorigenesis by TSAHC and sorafenib. Cancer Biol Ther 2011;11:330-336.
41. Lee SA, Kim TY, Kwak TK, Kim H, Kim S, Lee HJ, Kim SH, et al. Transmembrane 4 L

six family member 5 (TM4SF5) enhances migration and invasion of hepatocytes for effective metastasis. J Cell Biochem 2010;111:59-66.

42. Kang M, Ryu J, Lee D, Lee MS, Kim HJ, Nam SH, Song HE, et al. Correlations between Transmembrane 4 L6 family member 5 (TM4SF5), CD151, and CD63 in liver fibrotic phenotypes and hepatic migration and invasive capacities. PLoS ONE 2014;9:e102817.

## Figure Legends

**Fig. 1. TM4SF5 expression promoted spheroid formation in HCC. (A−C)** Spheroid formation assays showed that TM4SF5-expressing cells [Huh7, HepG2 (A), SNU449$T_p$, SNU449$T_3$, SNU449$T_7$, SNU449$T_{10}$, and SNU449$T_{16}$ clones (B)] exhibited enhanced sphere-forming capacities, compared to cells lacking TM4SF5 (SNU449 parental, P, and SNU449$C_p$ stable clone) or expressing the *N*-glycosylation TM4SF5 mutant [N138A, N155Q, and NANQ (N138A/N115Q)]. The images were saved 10 days after seeding cells into 6-well ultra-low attachment plates. Scale bars represent 70 μm (B). Spheroids larger than 70 μm were selected via sieving and counting (C). **(D)** Aldefluor assays were performed using spheroids larger than 70 μm. **(E and F)** Stable knockdown of endogenous TM4SF5 in Huh7 cells was done before analyses of spheroid formation (E) and TM4SF5-mediated downstream signaling activities (F). * depicts $p < 0.05$ for a statistical significance. The graphs show the spheroid numbers (C, F) or ALDH activity (D) at the mean ± standard deviation. All data are representative of three independent experiments.

**Fig. 2. TM4SF5 and CD44 appeared important for spheroid formation. (A)** mRNA levels were determined by RT-PCR from stable SNU449 cell clones. β-actin was used as a control. (**B**) Whole cell lysates from the cells were immunoblotted for the indicated molecules. **(C, D)** Flow cytometry analysis was performed for CD24 (B) and CD44 (C, upper panel using the

anti-CD44 antibody IM7 clone and lower panel using the DF1485 clone) expression in stable SNU449 cell clones. The black histograms indicate no secondary antibody controls. (**E**) Flow cytometry analysis was performed using the anti-CD44 DF1485 clone for CD44 expression in the SNU449 stable cell clones after 24 h DMSO or TSAHC (20 μM) treatment. TSAHC treated cells (red) and DMSO-treated cells (green) were compared with no secondary antibody controls (black field). **(F)** Stable SNU449 clones treated with DMSO or TSAHC (20 μM) for 24 h were processed for RT-PCR to analyze *CD44* and *β-actin* mRNA levels. The data represent three independent experiments.

**Fig. 3. Spheroid formation depending on the extracellular interaction between TM4SF5 and CD44.** (**A**−**C**) SNU449 parental cells were transfected with the indicated expression vectors for 48 h (A, B). DMSO (-) or 20 μM TSAHC (+) was treated for an additional 24 h (C). Whole cell lysates were prepared and pulled down using streptavidin-beads, prior to standard western blotting. (**D**) Flow cytometry analysis using the DF1485 antibody was performed for CD44 expression in Huh7 cells stably expressing shScramble (upper panels) or shTM4SF5 (lower panels). **(E)** Stable SNU449 clones (normal) or cells treated with DMSO or TSAHC (20 μM) were analyzed for spheroid formation. **(F)** Stable TM4SF5-expressing SNU449$T_7$ cells were stably transfected with shRNA against a scramble sequence (shScram) or CD44 (shCD44), before spheroid formation analysis for 10 days. The numbers of

spheroids (≥ 70 μm) are graphed at the mean ± SD. The data represent three independent experiments.

**Fig. 4. Self-renewal properties were controlled by TM4SF5 expression. (A, top graph and images)**. Representative images (inserts) showing the tumors formed by subcutaneous injection of stable SNU449 cell clones [TM4SF5-null SNU449$C_p$; $C_p$ (n = 5), TM4SF5 N138A/N155Q mutant-expressing SNU449 clone; NANQ (n = 5), $T_7$; and TM4SF5-expressing SNU449$T_7$ cells (n = 10)] using less than 5,000 cells/injection site. Tumors were formed only in SNU449$T_7$ cell-injected flanks, as shown in the graphs of different cell numbers per injection site. TM4SF5-null or mutant cells were not shown due to no tumor formation. The tumor volumes were reported as the mean ± SD values for each number of SNU449$T_7$ cells injected. **(A, middle immunoblots)** SNU449$C_p$ ($C_p$), SNU449$T_7$, or Exp$T_7$ cells [prepared from xenograft tissues (mouse #2 and #3)] were harvested for standard western blotting (middle). **(A, bottom spheroid images)** Spheroid formation was compared for SNU449$T_7$ and Exp$T_{7\text{-}2}$ for 10 days (bottom). **(B, top graph)** Tumor volumes (n = 7) resulting from the subcutaneous injection of Exp$T_{7\text{-}2}$ (i.e., the cells prepared from the xenograft tumors after SNU449$T_7$ cell injection), as shown in the graphs at different cell numbers per injection site. TM4SF5-null or mutant cells were not shown due to no tumor formation. Tumor volumes were reported as the mean ± SD values. **(B, bottom**

**immunoblots)** SNU449$C_p$ ($C_p$), SNU449$T_7$ ($T_7$), Exp$T_{7\text{-}2}$, and the secondary explants ($^{2nd}$Exp$T_{7\text{-}2}$, the cells prepared from the xenograft tumors after Exp$T_{7\text{-}2}$ cell injection) were harvested for standard western blotting. **(C)** The primary xenograft tumor sections after injection of SNU449$_{T7}$ were stained with DAPI (blue) and immunostained for CD44 (red) and TM4SF5 (green). Regions from three different mice are shown with enlargement at right. **(D)** FACS analysis using SNU449$T_7$, Exp$T_{7\text{-}2}$, and Exp$T_{7\text{-}3}$ cells was performed for CD44 (using clone IM7 antibody), TM4SF5, CD24, CD90, and CD133. **(E)** FACS analysis with double staining (with anti-CD44 clone IM7 and anti-TM4SF5[42] antibody) was performed for the indicated cells. The data shown represent three independent experiments.

**Fig. 5. TM4SF5 regulated c-Src, STAT3, Twist1, and Bmi1 for the self-renewal property.** (**A**) Stable cells were harvested for standard western blotting or processed for RT-PCR. **(B, C)** SNU449$T_7$ cells stably transfected with shScram, shTM4SF5, or shCD44 were harvested as whole cells lysates before standard western blotting. **(D)** Serial sections (6 μm) from xenograft tissues injected with SNU449$T_7$ (mouse #2 and #3) were immunostained for the molecules. The magnifications shown are 100× and 400×. **(E)** Stable cells expressing TM4SF5 were treated with DMSO or TSAHC (20 μM) for 24 h, then harvested as whole cell extracts, before standard western blotting or RT-PCR analysis. **(F)** Huh7 cells (normal) or cells treated with DMSO or TSAHC (20 μM) were examined for spheroid formation (top),

and then harvested for standard western blotting or RT-PCR (bottom). The data represent three different experiments.

**Fig. 6. TM4SF5-dependent c-Src, STAT3, and Bmi1 signaling was required for the self-renewal property. (A, B)** Spheroid formation was evaluated in stable SNU449 clones treated with either DMSO, specific c-Src inhibitor PP2, or negative control compound PP3 (A) or treated with either DMSO or STAT3 inhibitor (STATtic) at various concentrations (B). **(C, D)** Cells were transiently transfected with Bmi1 expression vector (C) or shRNA against Bmi1 (shBmi1, D) for 48 h and enriched under a selective pressure using G418 (250 μg/ml) for 1 week, before western blotting or spheroid forming assays. **(E)** Serial sections of tumor tissues from clinical HCC patients were processed for immunohistochemistry using normal mouse or rabbit IgG, TM4SF5, CD44, or Bmi1 antibody. The black boxes indicate the enlarged areas that are shown directly below. The magnifications shown are 100× and 400×. The data represent three different experiments.

**Fig. 7. Identification of TM4SF5-dependent CTCs and their metastasis.** SNU449$T_7$ cells stably transfected with tGFP-shScram or tGFP-shTM4SF5 were orthotopically injected into livers (500,000 cells/mouse for 4 weeks or 200,000 cells/mouse for 6 weeks); separate injections of PBS alone were also performed as controls. **(A)** Four weeks later, blood samples

collected from each mouse (middle images) were processed for FACS sorting (left histograms) and then seeded onto fibronectin-coated (10 μg/ml) coverslips prior to visualizing for tGFP (green) and staining with anti-tGFP antibody (red) or DAPI (blue). **(B)** The numbers of CTC-like cells sorted from the blood samples of mice injected with PBS (n = 5) were graphed at the mean ± SD, using SNU449$T_7$-tGFP-shScram cells (n = 10) or SNU449$T_7$-tGFP-shTM4SF5 cells (n = 5). **(C)** Mice orthotopically injected with SNU449$T_7$-tGFP-shScram (n = 3) or SNU449$T_7$-tGFP-shTM4SF5 (n = 3) were processed for CTC imaging using confocal laser endomicroscopy 6 weeks after the injection. Sections of blood vessels (0.453 $mm^2$) from each mouse were imaged for 20 min. **(D)** Mice orthotopically injected with vehicle (PBS, n = 2), SNU449$T_7$-shScram cells (n = 7), or SNU449$T_7$-shCD44 cells (n = 7) for 6 weeks were processed for collection of blood samples and the analysis of survival, and then the blood samples were processed and visualized using a fluorescent microscope after DAPI staining. The data represent three independent experiments.

**Fig. 8. Anti-TM4SF5 reagent blocked metastasis of orthotopically liver-injected cells to intestines. (A−E)** Mice orthotopically liver-injected with SNU449$T_7$-pMSCV-Luc2 cells were treated with either DMSO or TSAHC, as explained in the Experimental Procedures. **(A)** Upto 2 weeks after the cell injection and treatment, bioluminescence images were saved. Mice marked with red rectangles depict mice with metastasized tumors. **(B)** The total

bioluminescence flux after 3 week treatment were measured and shown as the mean ± SD. **(C)** Representative images of tumors in mouse treated with DMSO or TSAHC for 3 weeks. **(D)** Total flux (left) or number of metastatic tumors (right) was measured, and presented as the mean ± SD. $p \geq 0.05$ or $p < 0.05$ depicts statistical insignificance or significance, respectively. **(E)** Orthotopic tumors or metastatic tumors at the intestine or peritoneal membrane (Mem) were counted after abdominal surgery from each mouse treated with DMSO (n = 8) or TSAHC (n = 8) and graphed as the mean ± SD. The data represent three independent experiments. **(F)** Schematic model for TM4SF5-induced self-renewal capacity leading to CTC and liver-to-intestine metastases.

Figure 1 (LEE)

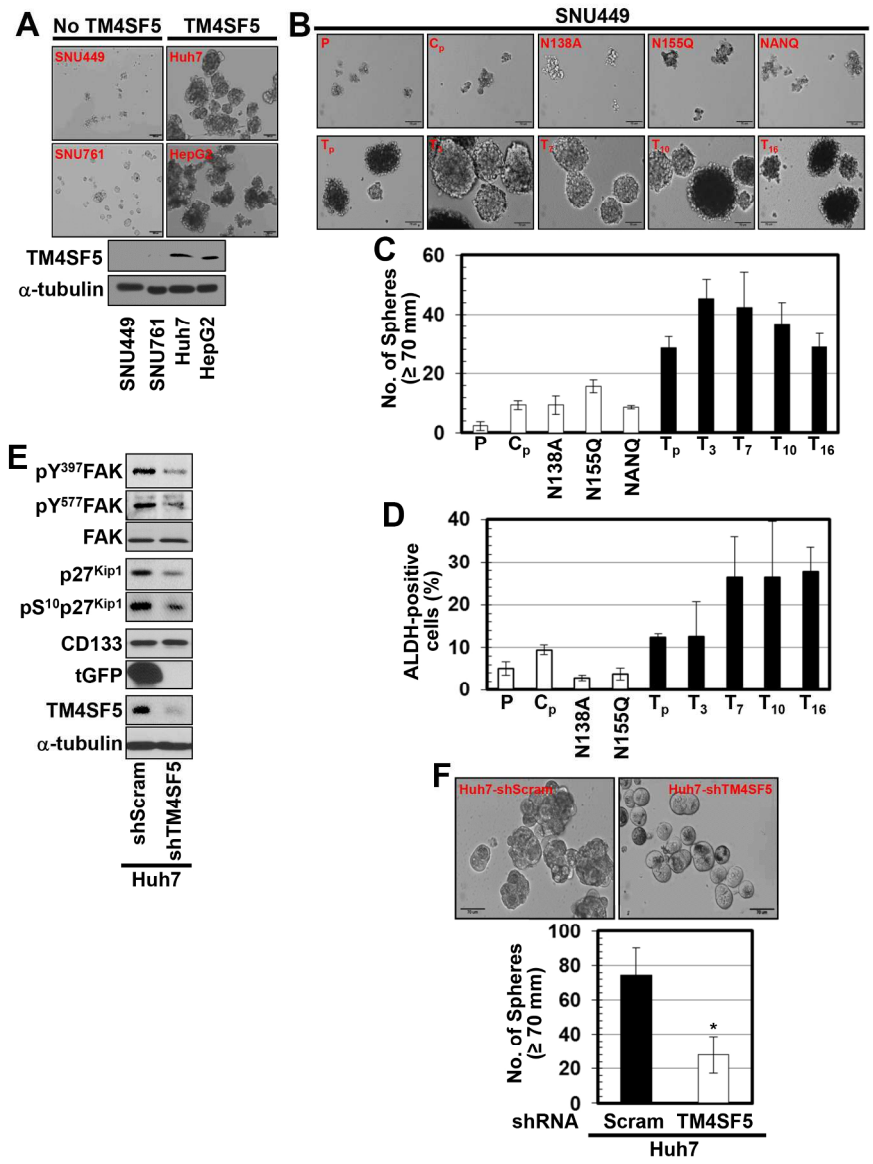


Fig. 1. TM4SF5 expression promoted spheroid formation in HCC. (A–C) Spheroid formation assays showed that TM4SF5-expressing cells [Huh7, HepG2 (A), SNU449$T_p$, SNU449$T_3$, SNU449$T_7$, SNU449$T_{10}$, and SNU449$T_{16}$ clones (B)] exhibited enhanced sphere-forming capacities, compared to cells lacking TM4SF5 (SNU449 parental, P, and SNU449$C_p$ stable clone) or expressing the N-glycosylation TM4SF5 mutant [N138A, N155Q, and NANQ (N138A/N115Q)]. The images were saved 10 days after seeding cells into 6-well ultra-low attachment plates. Scale bars represent 70 μm (B). Spheroids larger than 70 μm were selected via sieving and counting (C). (D) Aldefluor assays were performed using spheroids larger than 70 μm. (E and F) Stable knockdown of endogenous TM4SF5 in Huh7 cells was done before analyses of spheroid formation (E) and TM4SF5-mediated downstream signaling activities (F). * depicts $p < 0.05$ for a statistical significance. The graphs show the spheroid numbers (C, F) or ALDH activity (D) at the mean ± standard deviation. All data are representative of three independent experiments.
187x254mm (300 x 300 DPI)

Figure 2 (LEE)

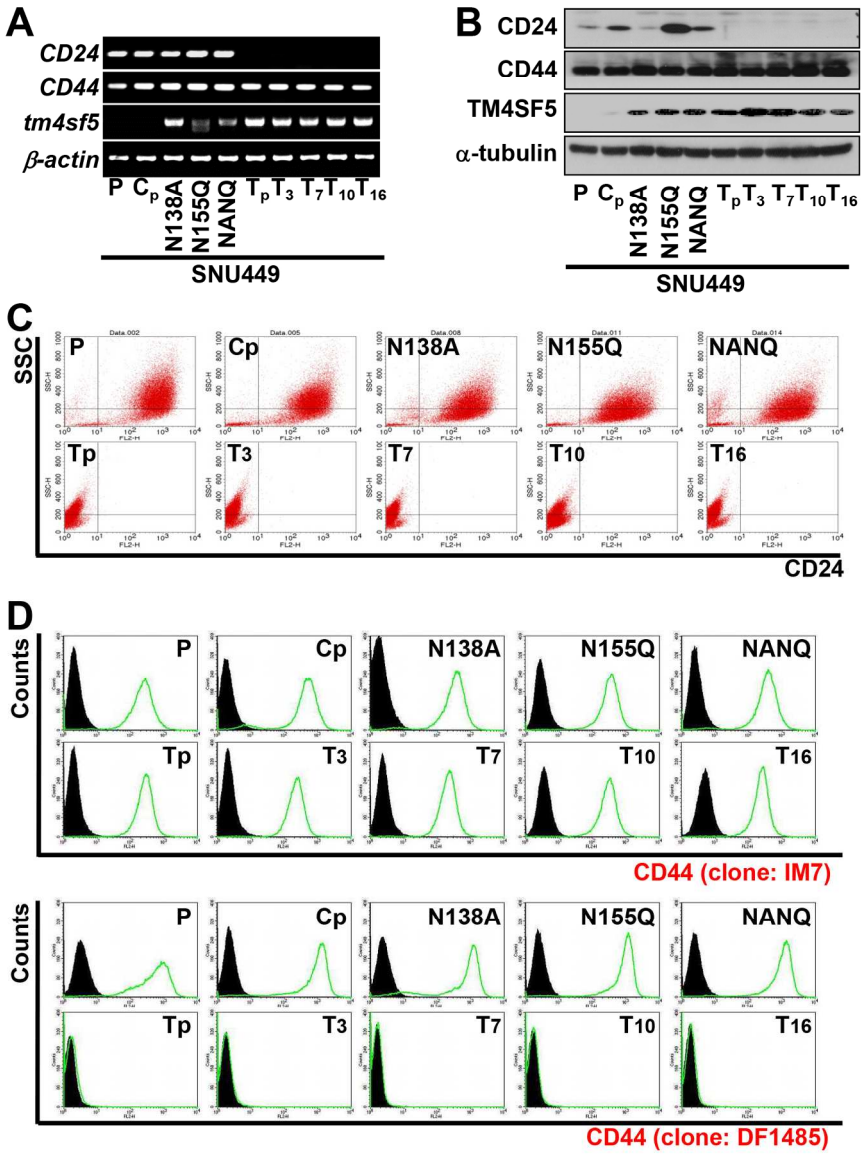


Fig. 2. TM4SF5 and CD44 appeared important for spheroid formation. (A) mRNA levels were determined by RT-PCR from stable SNU449 cell clones. β-actin was used as a control. (B) Whole cell lysates from the cells were immunoblotted for the indicated molecules. (C, D) Flow cytometry analysis was performed for CD24 (B) and CD44 (C, upper panel using the anti-CD44 antibody IM7 clone and lower panel using the DF1485 clone) expression in stable SNU449 cell clones. The black histograms indicate no secondary antibody controls. (E) Flow cytometry analysis was performed using the anti-CD44 DF1485 clone for CD44 expression in the SNU449 stable cell clones after 24 h DMSO or TSAHC (20 μM) treatment. TSAHC treated cells (red) and DMSO-treated cells (green) were compared with no secondary antibody controls (black field). (F) Stable SNU449 clones treated with DMSO or TSAHC (20 μM) for 24 h were processed for RT-PCR to analyze *CD44* and *β-actin* mRNA levels. The data represent three independent experiments.
158x214mm (300 x 300 DPI)

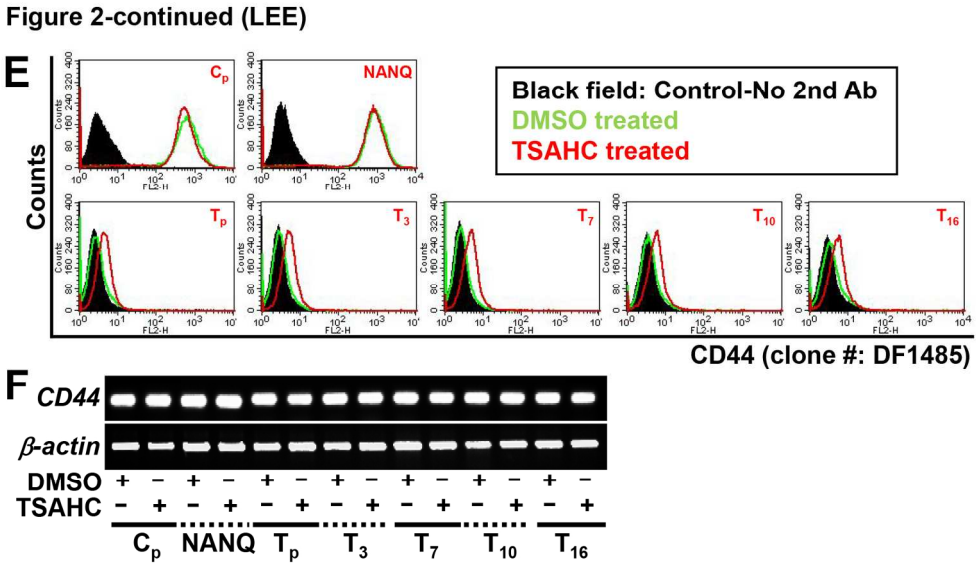


Fig. 2. TM4SF5 and CD44 appeared important for spheroid formation. (A) mRNA levels were determined by RT-PCR from stable SNU449 cell clones. β-actin was used as a control. (B) Whole cell lysates from the cells were immunoblotted for the indicated molecules. (C, D) Flow cytometry analysis was performed for CD24 (B) and CD44 (C, upper panel using the anti-CD44 antibody IM7 clone and lower panel using the DF1485 clone) expression in stable SNU449 cell clones. The black histograms indicate no secondary antibody controls. (E) Flow cytometry analysis was performed using the anti-CD44 DF1485 clone for CD44 expression in the SNU449 stable cell clones after 24 h DMSO or TSAHC (20 μM) treatment. TSAHC treated cells (red) and DMSO-treated cells (green) were compared with no secondary antibody controls (black field). (F) Stable SNU449 clones treated with DMSO or TSAHC (20 μM) for 24 h were processed for RT-PCR to analyze *CD44* and *β-actin* mRNA levels. The data represent three independent experiments.
167x97mm (300 x 300 DPI)

Figure 3 (LEE)

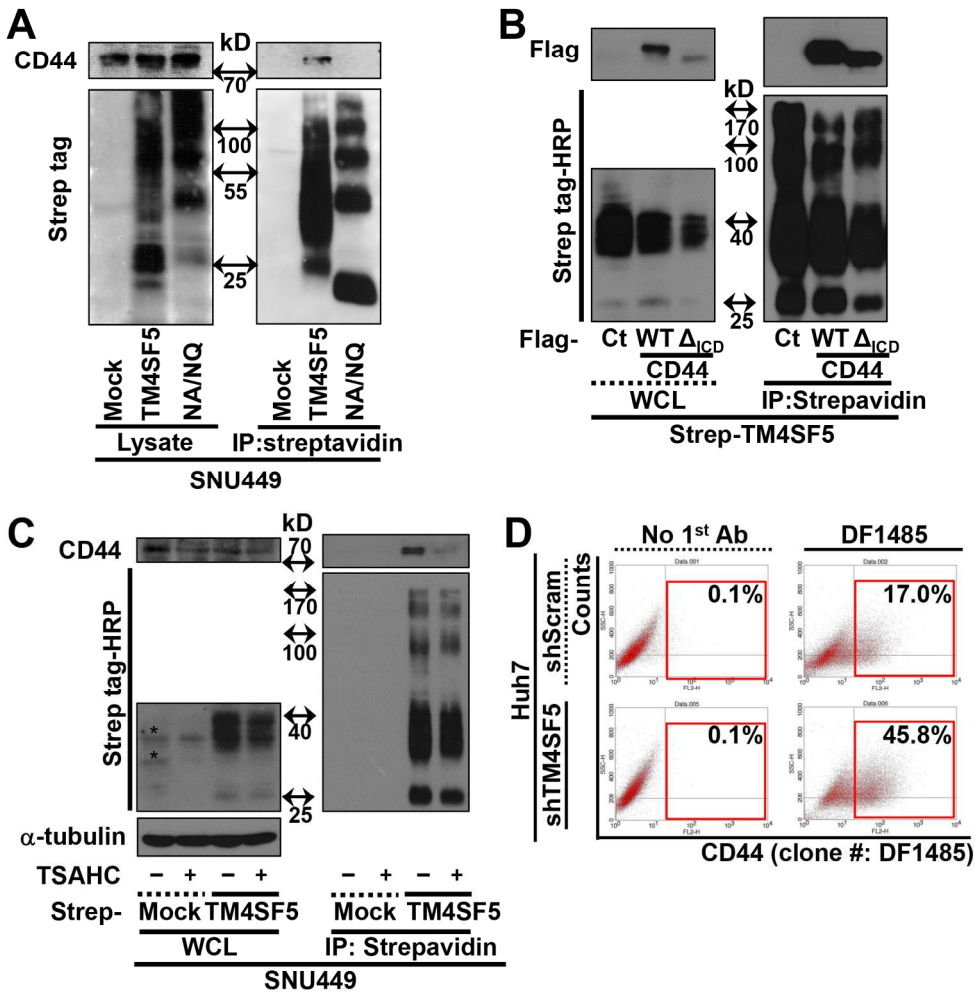


Fig. 3. Spheroid formation depending on the extracellular interaction between TM4SF5 and CD44. (A–C) SNU449 parental cells were transfected with the indicated expression vectors for 48 h (A, B). DMSO (-) or 20 μM TSAHC (+) was treated for an additional 24 h (C). Whole cell lysates were prepared and pulled down using streptavidin-beads, prior to standard western blotting. (D) Flow cytometry analysis using the DF1485 antibody was performed for CD44 expression in Huh7 cells stably expressing shScramble (upper panels) or shTM4SF5 (lower panels). (E) Stable SNU449 clones (normal) or cells treated with DMSO or TSAHC (20 μM) were analyzed for spheroid formation. (F) Stable TM4SF5-expressing SNU449$T_7$ cells were stably transfected with shRNA against a scramble sequence (shScram) or CD44 (shCD44), before spheroid formation analysis for 10 days. The numbers of spheroids (≥ 70 μm) are graphed at the mean ± SD. The data represent three independent experiments.
172x181mm (300 x 300 DPI)

Figure 3-continued (LEE)

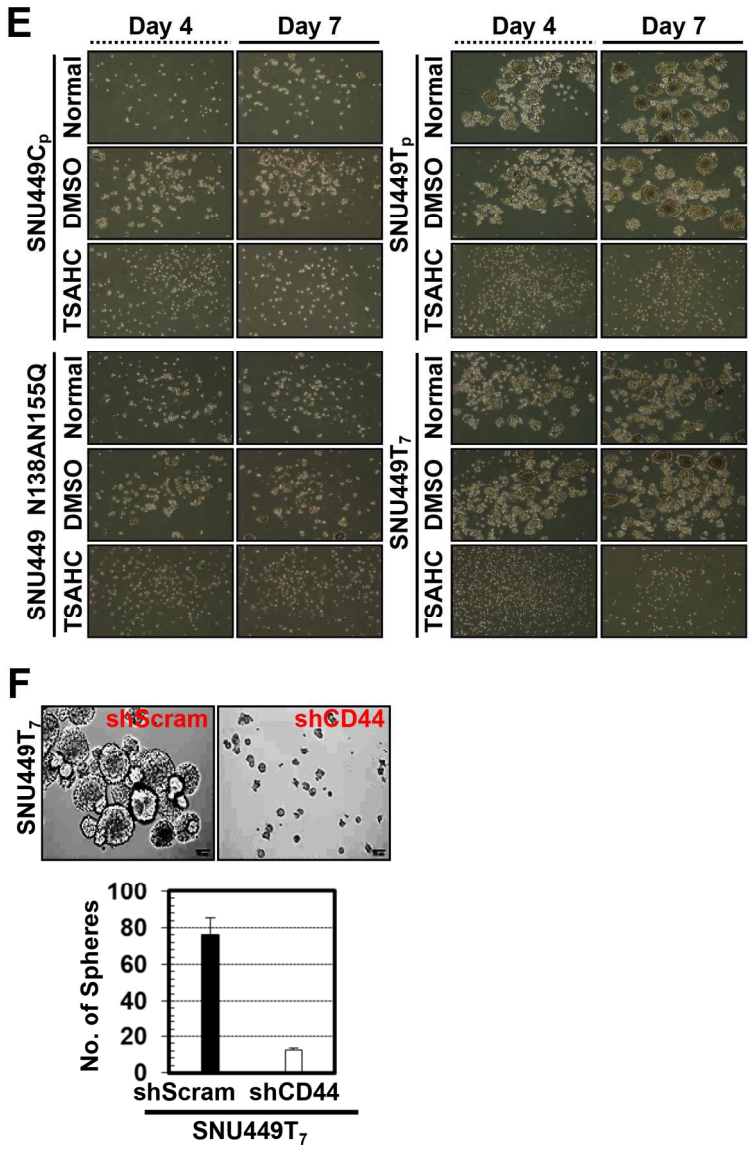


Fig. 3. Spheroid formation depending on the extracellular interaction between TM4SF5 and CD44. (A–C) SNU449 parental cells were transfected with the indicated expression vectors for 48 h (A, B). DMSO (-) or 20 μM TSAHC (+) was treated for an additional 24 h (C). Whole cell lysates were prepared and pulled down using streptavidin-beads, prior to standard western blotting. (D) Flow cytometry analysis using the DF1485 antibody was performed for CD44 expression in Huh7 cells stably expressing shScramble (upper panels) or shTM4SF5 (lower panels). (E) Stable SNU449 clones (normal) or cells treated with DMSO or TSAHC (20 μM) were analyzed for spheroid formation. (F) Stable TM4SF5-expressing SNU449T$_7$ cells were stably transfected with shRNA against a scramble sequence (shScram) or CD44 (shCD44), before spheroid formation analysis for 10 days. The numbers of spheroids (≥ 70 μm) are graphed at the mean ± SD. The data represent three independent experiments.
134x208mm (300 x 300 DPI)

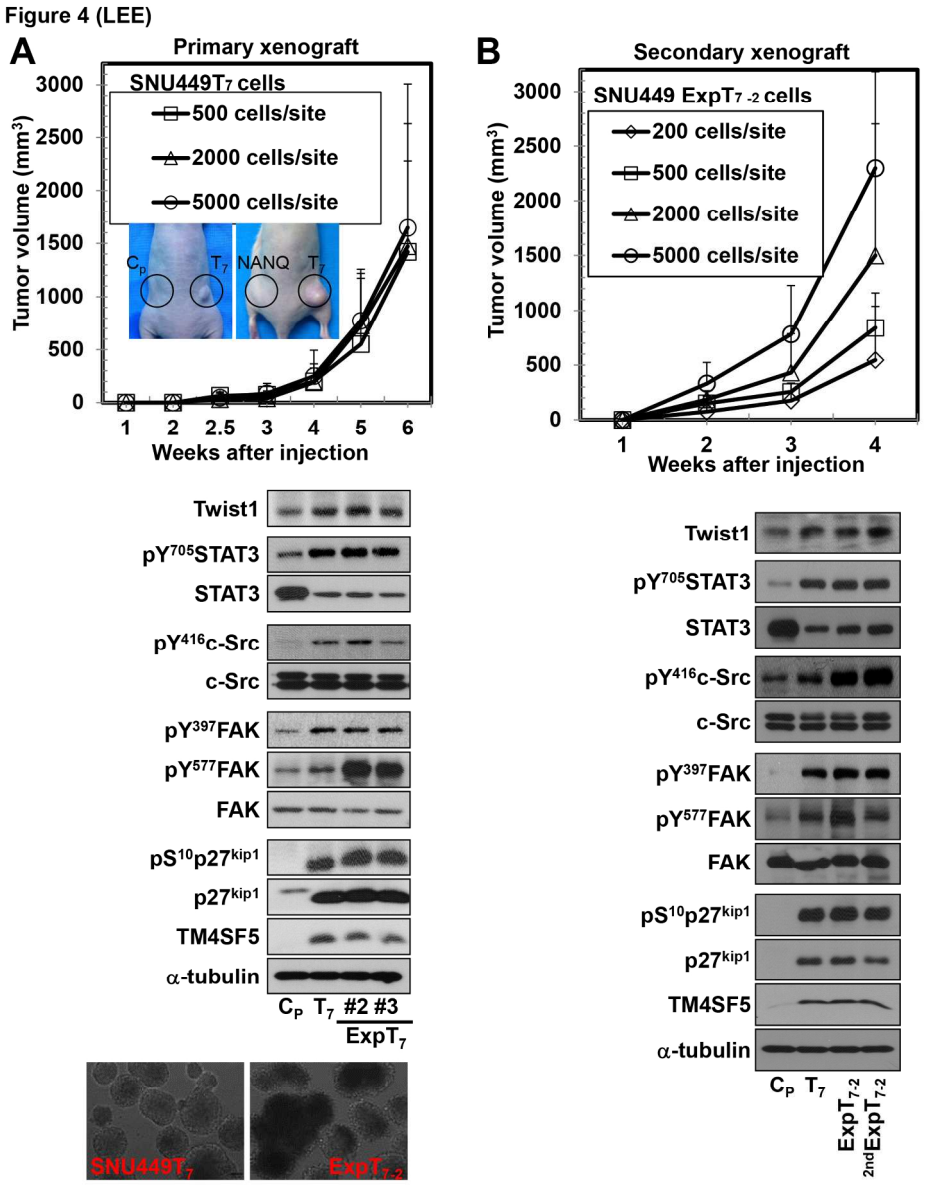


Fig. 4. Self-renewal properties were controlled by TM4SF5 expression. (A, top graph and images). Representative images (inserts) showing the tumors formed by subcutaneous injection of stable SNU449 cell clones [TM4SF5-null SNU449$C_p$; $C_p$ (n = 5), TM4SF5 N138A/N155Q mutant-expressing SNU449 clone; NANQ (n = 5), $T_7$; and TM4SF5-expressing SNU449$T_7$ cells (n = 10)] using less than 5,000 cells/injection site. Tumors were formed only in SNU449$T_7$ cell-injected flanks, as shown in the graphs of different cell numbers per injection site. TM4SF5-null or mutant cells were not shown due to no tumor formation. The tumor volumes were reported as the mean ± SD values for each number of SNU449$T_7$ cells injected. (A, middle immunoblots) SNU449$C_p$ ($C_p$), SNU449$T_7$, or Exp$T_7$ cells [prepared from xenograft tissues (mouse #2 and #3)] were harvested for standard western blotting (middle). (A, bottom spheroid images) Spheroid formation was compared for SNU449$T_7$ and Exp$T_{7\text{-}2}$ for 10 days (bottom). (B, top graph) Tumor volumes (n = 7) resulting from the subcutaneous injection of Exp$T_{7\text{-}2}$ (i.e., the cells prepared from the xenograft tumors after SNU449$T_7$ cell injection), as shown in the graphs at different cell numbers per injection site. TM4SF5-null or mutant cells were not shown due to no tumor formation. Tumor volumes were reported as the mean

± SD values. (B, bottom immunoblots) SNU449$C_D$ ($C_D$), SNU449$T_7$ ($T_7$), Exp$T_{7\text{-}2}$, and the secondary explants ($^{2nd}$Exp$T_{7\text{-}2}$, the cells prepared from the xenograft tumors after Exp$T_{7\text{-}2}$ cell injection) were harvested for standard western blotting. (C) The primary xenograft tumor sections after injection of SNU449$T_7$ were stained with DAPI (blue) and immunostained for CD44 (red) and TM4SF5 (green). Regions from three different mice are shown with enlargement at right. (D) FACS analysis using SNU449$T_7$, Exp$T_{7\text{-}2}$, and Exp$T_{7\text{-}3}$ cells was performed for CD44 (using clone IM7 antibody), TM4SF5, CD24, CD90, and CD133. (E) FACS analysis with double staining (with anti-CD44 clone IM7 and anti-TM4SF5[42] antibody) was performed for the indicated cells. The data shown represent three independent experiments.
181x233mm (300 x 300 DPI)

Figure 4-continued (LEE)

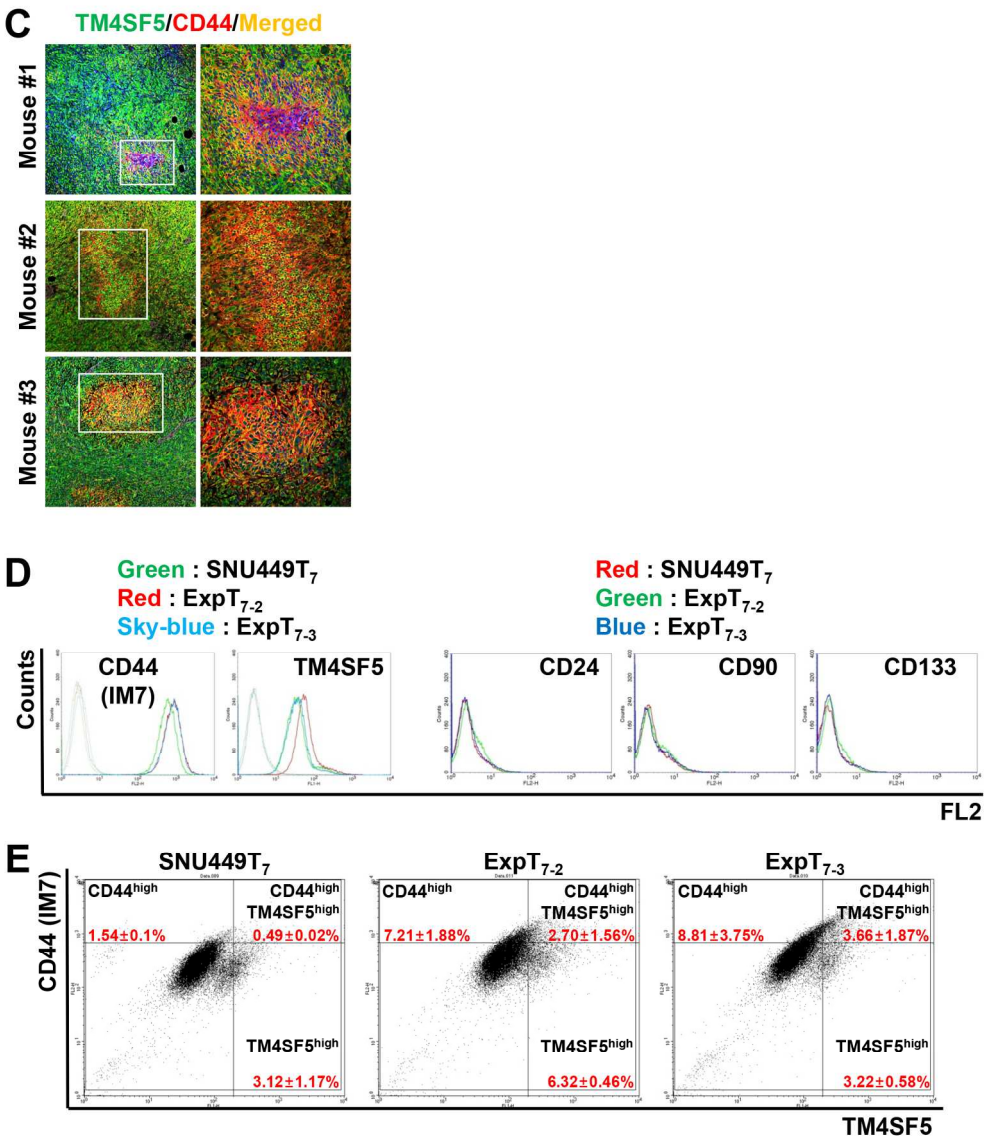


Fig. 4. Self-renewal properties were controlled by TM4SF5 expression. (A, top graph and images). Representative images (inserts) showing the tumors formed by subcutaneous injection of stable SNU449 cell clones [TM4SF5-null SNU449$C_p$; $C_p$ (n = 5), TM4SF5 N138A/N155Q mutant-expressing SNU449 clone; NANQ (n = 5), $T_7$; and TM4SF5-expressing SNU449$T_7$ cells (n = 10)] using less than 5,000 cells/injection site. Tumors were formed only in SNU449$T_7$ cell-injected flanks, as shown in the graphs of different cell numbers per injection site. TM4SF5-null or mutant cells were not shown due to no tumor formation. The tumor volumes were reported as the mean ± SD values for each number of SNU449$T_7$ cells injected. (A, middle immunoblots) SNU449$C_p$ ($C_p$), SNU449$T_7$, or Exp$T_7$ cells [prepared from xenograft tissues (mouse #2 and #3)] were harvested for standard western blotting (middle). (A, bottom spheroid images) Spheroid formation was compared for SNU449$T_7$ and Exp$T_{7-2}$ for 10 days (bottom). (B, top graph) Tumor volumes (n = 7) resulting from the subcutaneous injection of Exp$T_{7-2}$ (i.e., the cells prepared from the xenograft tumors after SNU449$T_7$ cell injection), as shown in the graphs at different cell numbers per injection site. TM4SF5-null or mutant cells were not shown due to no tumor formation. Tumor volumes were reported as the mean

± SD values. (B, bottom immunoblots) SNU449$C_D$ ($C_D$), SNU449$T_7$ ($T_7$), Exp$T_{7\text{-}2}$, and the secondary explants ($^{2nd}$Exp$T_{7\text{-}2}$, the cells prepared from the xenograft tumors after Exp$T_{7\text{-}2}$ cell injection) were harvested for standard western blotting. (C) The primary xenograft tumor sections after injection of SNU449$T_7$ were stained with DAPI (blue) and immunostained for CD44 (red) and TM4SF5 (green). Regions from three different mice are shown with enlargement at right. (D) FACS analysis using SNU449$T_7$, Exp$T_{7\text{-}2}$, and Exp$T_{7\text{-}3}$ cells was performed for CD44 (using clone IM7 antibody), TM4SF5, CD24, CD90, and CD133. (E) FACS analysis with double staining (with anti-CD44 clone IM7 and anti-TM4SF5[42] antibody) was performed for the indicated cells. The data shown represent three independent experiments.
179x214mm (300 x 300 DPI)

Figure 5 (LEE)

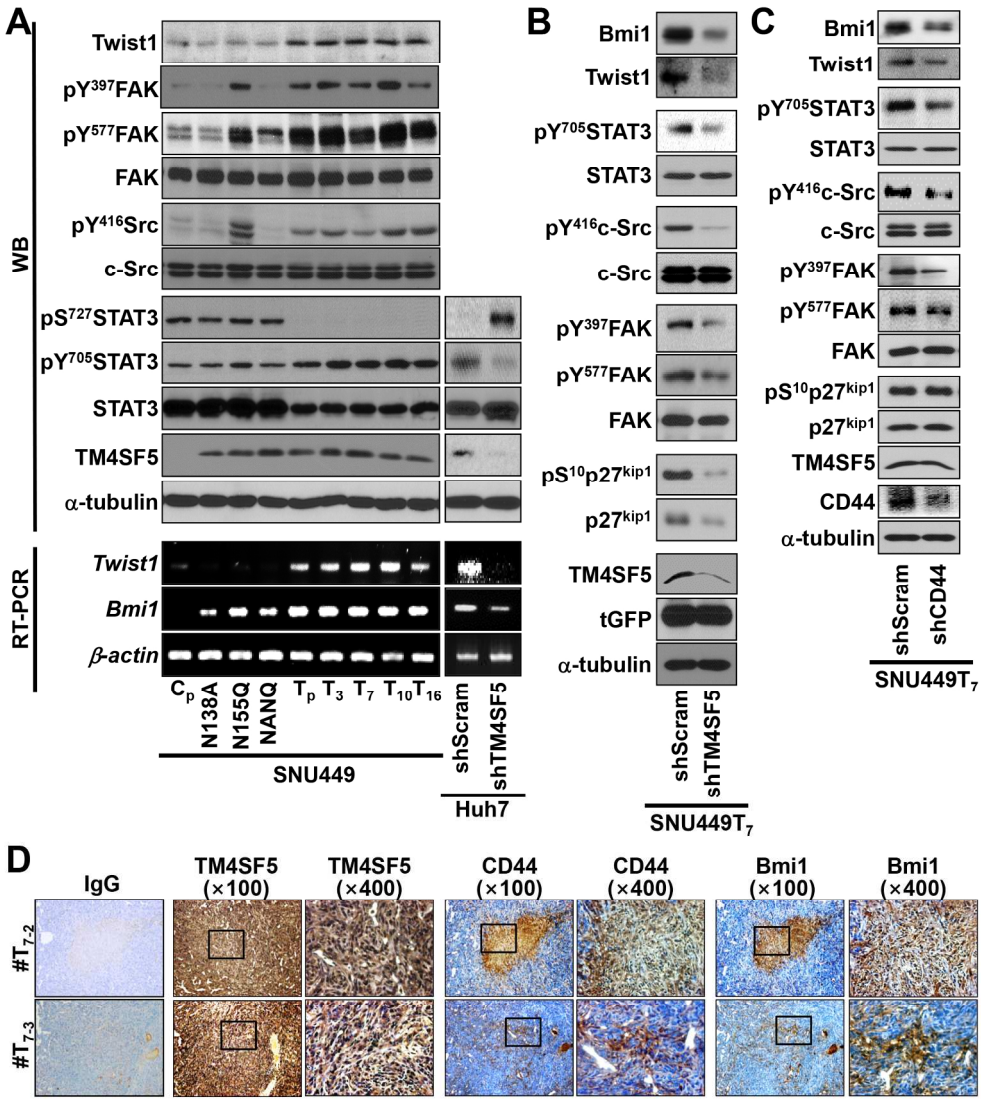


Fig. 5. TM4SF5 regulated c-Src, STAT3, Twist1, and Bmi1 for the self-renewal property. (A) Stable cells were harvested for standard western blotting or processed for RT-PCR. (B, C) SNU449$T_7$ cells stably transfected with shScram, shTM4SF5, or shCD44 were harvested as whole cells lysates before standard western blotting. (D) Serial sections (6 μm) from xenograft tissues injected with SNU449T7 (mouse #2 and #3) were immunostained for the molecules. The magnifications shown are 100× and 400×. (E) Stable cells expressing TM4SF5 were treated with DMSO or TSAHC (20 μM) for 24 h, then harvested as whole cell extracts, before standard western blotting or RT-PCR analysis. (F) Huh7 cells (normal) or cells treated with DMSO or TSAHC (20 μM) were examined for spheroid formation (top), and then harvested for standard western blotting or RT-PCR (bottom). The data represent three different experiments.
193x222mm (300 x 300 DPI)

Figure 5-continued (LEE)

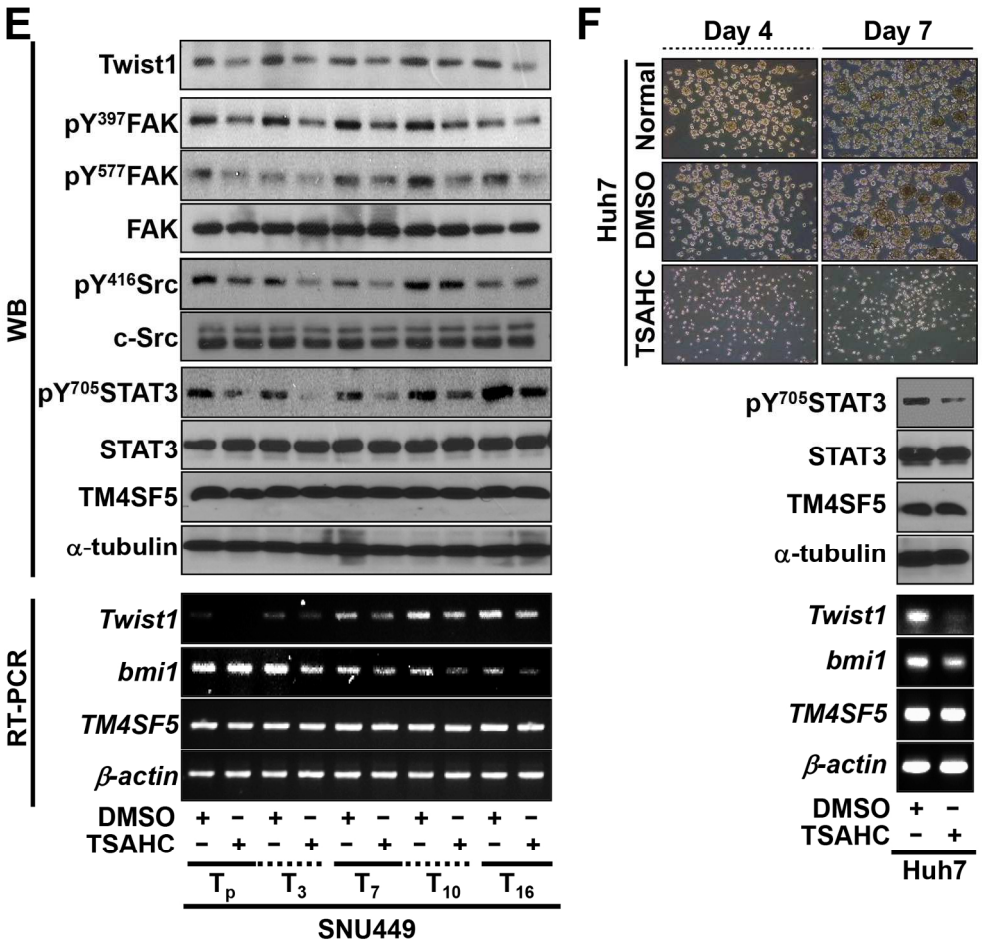


Fig. 5. TM4SF5 regulated c-Src, STAT3, Twist1, and Bmi1 for the self-renewal property. (A) Stable cells were harvested for standard western blotting or processed for RT-PCR. (B, C) SNU449$T_7$ cells stably transfected with shScram, shTM4SF5, or shCD44 were harvested as whole cells lysates before standard western blotting. (D) Serial sections (6 μm) from xenograft tissues injected with SNU449T7 (mouse #2 and #3) were immunostained for the molecules. The magnifications shown are 100× and 400×. (E) Stable cells expressing TM4SF5 were treated with DMSO or TSAHC (20 μM) for 24 h, then harvested as whole cell extracts, before standard western blotting or RT-PCR analysis. (F) Huh7 cells (normal) or cells treated with DMSO or TSAHC (20 μM) were examined for spheroid formation (top), and then harvested for standard western blotting or RT-PCR (bottom). The data represent three different experiments.
162x162mm (300 x 300 DPI)

Figure 6 (LEE)

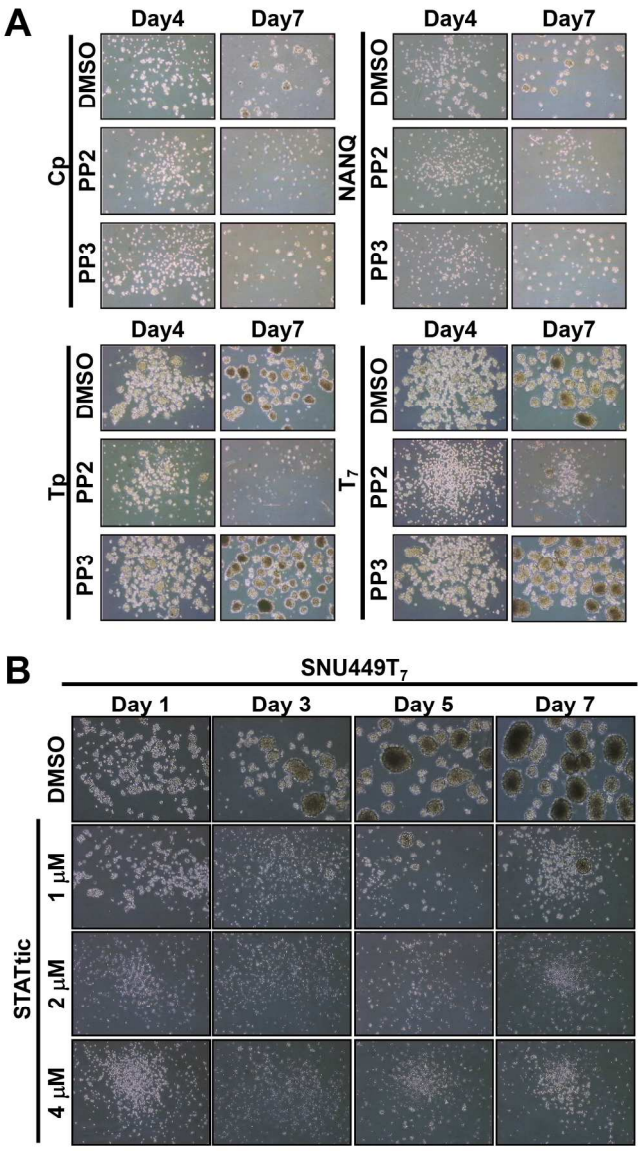


Fig. 6. TM4SF5-dependent c-Src, STAT3, and Bmi1 signaling was required for the self-renewal property. (A, B) Spheroid formation was evaluated in stable SNU449 clones treated with either DMSO, specific c-Src inhibitor PP2, or negative control compound PP3 (A) or treated with either DMSO or STAT3 inhibitor (STATtic) at various concentrations (B). (C, D) Cells were transiently transfected with Bmi1 expression vector (C) or shRNA against Bmi1 (shBmi1, D) for 48 h and enriched under a selective pressure using G418 (250 μg/ml) for 1 week, before western blotting or spheroid forming assays. (E) Serial sections of tumor tissues from clinical HCC patients were processed for immunohistochemistry using normal mouse or rabbit IgG, TM4SF5, CD44, or Bmi1 antibody. The black boxes indicate the enlarged areas that are shown directly below. The magnifications shown are 100× and 400×. The data represent three different experiments.
123x224mm (300 x 300 DPI)

**Figure 6-continued (LEE)**

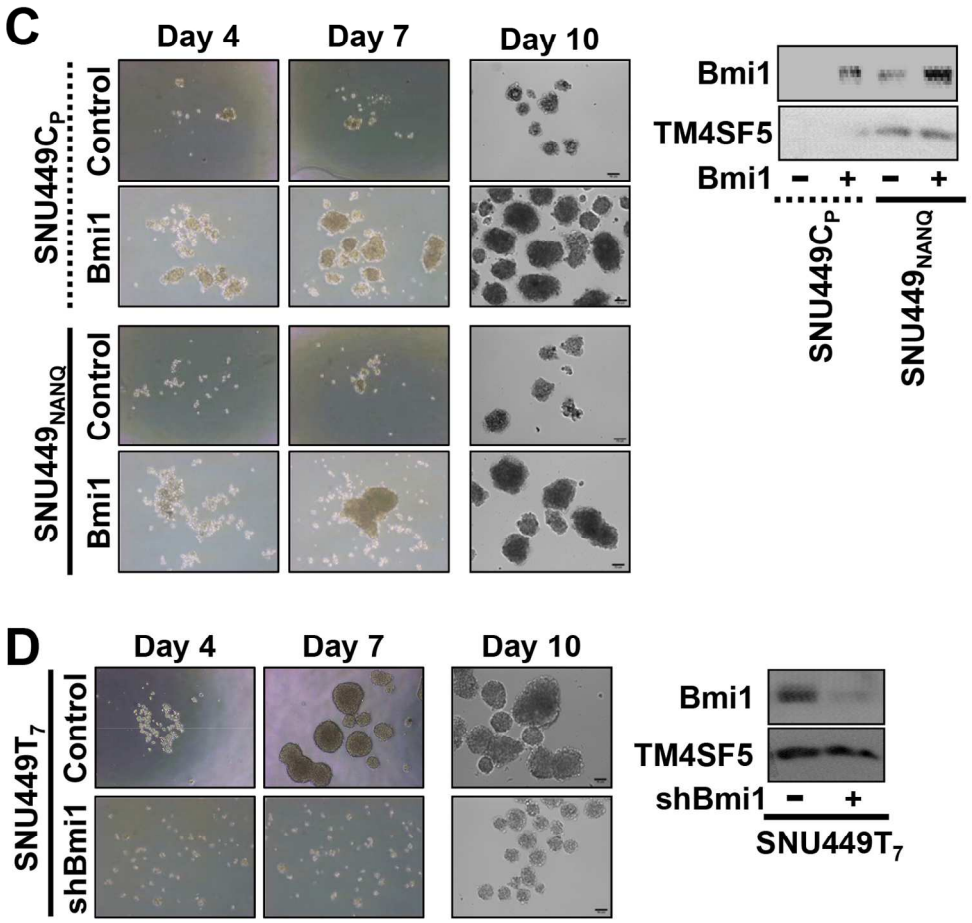


Fig. 6. TM4SF5-dependent c-Src, STAT3, and Bmi1 signaling was required for the self-renewal property. (A, B) Spheroid formation was evaluated in stable SNU449 clones treated with either DMSO, specific c-Src inhibitor PP2, or negative control compound PP3 (A) or treated with either DMSO or STAT3 inhibitor (STATtic) at various concentrations (B). (C, D) Cells were transiently transfected with Bmi1 expression vector (C) or shRNA against Bmi1 (shBmi1, D) for 48 h and enriched under a selective pressure using G418 (250 μg/ml) for 1 week, before western blotting or spheroid forming assays. (E) Serial sections of tumor tissues from clinical HCC patients were processed for immunohistochemistry using normal mouse or rabbit IgG, TM4SF5, CD44, or Bmi1 antibody. The black boxes indicate the enlarged areas that are shown directly below. The magnifications shown are 100× and 400×. The data represent three different experiments.
135x134mm (300 x 300 DPI)

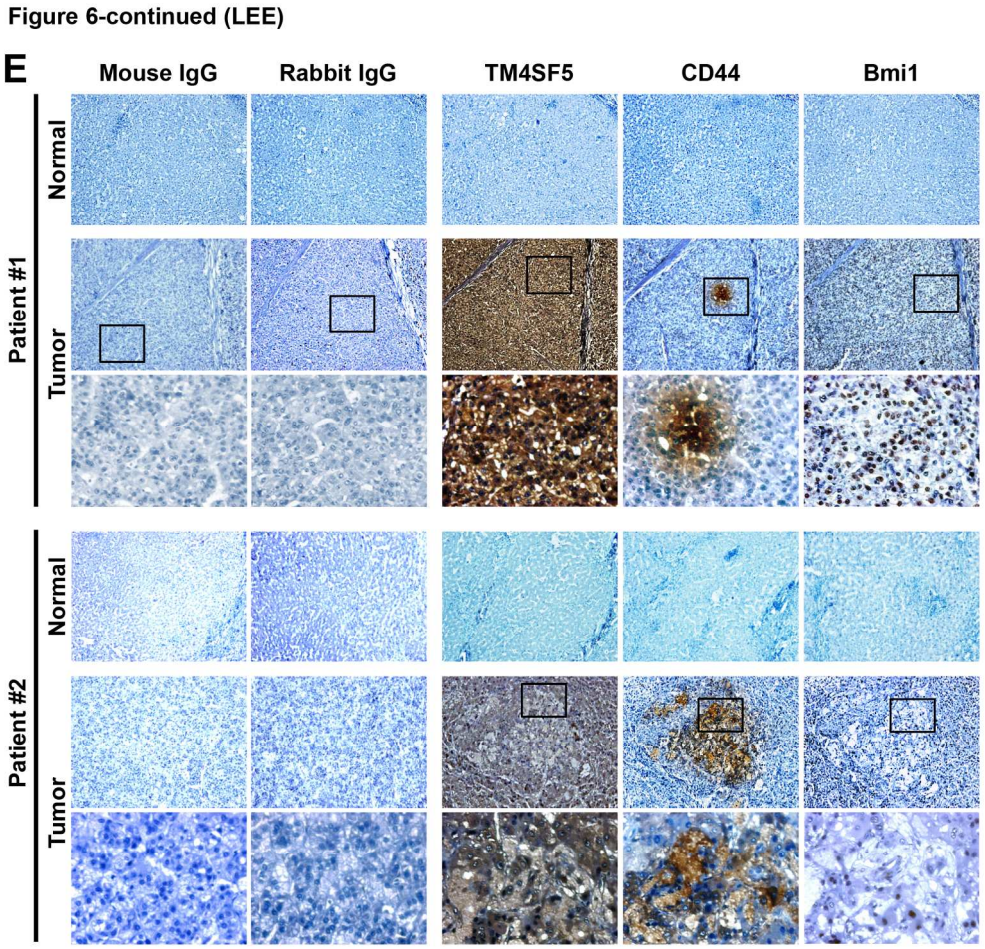


Fig. 6. TM4SF5-dependent c-Src, STAT3, and Bmi1 signaling was required for the self-renewal property. (A, B) Spheroid formation was evaluated in stable SNU449 clones treated with either DMSO, specific c-Src inhibitor PP2, or negative control compound PP3 (A) or treated with either DMSO or STAT3 inhibitor (STATtic) at various concentrations (B). (C, D) Cells were transiently transfected with Bmi1 expression vector (C) or shRNA against Bmi1 (shBmi1, D) for 48 h and enriched under a selective pressure using G418 (250 μg/ml) for 1 week, before western blotting or spheroid forming assays. (E) Serial sections of tumor tissues from clinical HCC patients were processed for immunohistochemistry using normal mouse or rabbit IgG, TM4SF5, CD44, or Bmi1 antibody. The black boxes indicate the enlarged areas that are shown directly below. The magnifications shown are 100× and 400×. The data represent three different experiments.
182x175mm (300 x 300 DPI)

Figure 7 (LEE)

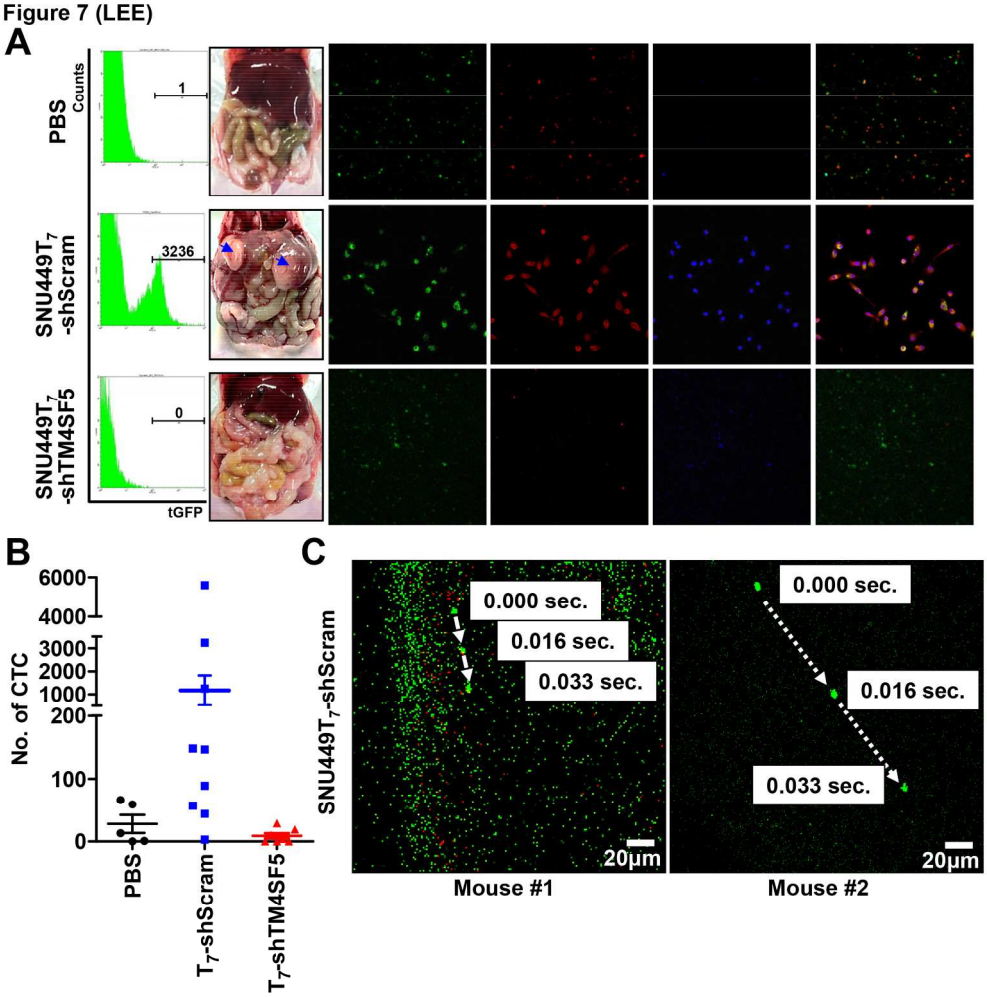


Fig. 7. Identification of TM4SF5-dependent CTCs and their metastasis. SNU449$T_7$ cells stably transfected with tGFP-shScram or tGFP-shTM4SF5 were orthotopically injected into livers (500,000 cells/mouse for 4 weeks or 200,000 cells/mouse for 6 weeks); separate injections of PBS alone were also performed as controls. (A) Four weeks later, blood samples collected from each mouse (middle images) were processed for FACS sorting (left histograms) and then seeded onto fibronectin-coated (10 μg/ml) coverslips prior to visualizing for tGFP (green) and staining with anti-tGFP antibody (red) or DAPI (blue). (B) The numbers of CTC-like cells sorted from the blood samples of mice injected with PBS (n = 5) were graphed at the mean ± SD, using SNU449$T_7$-tGFP-shScram cells (n = 10) or SNU449$T_7$-tGFP-shTM4SF5 cells (n = 5). (C) Mice orthotopically injected with SNU449$T_7$-tGFP-shScram (n = 3) or SNU449$T_7$-tGFP-shTM4SF5 (n = 3) were processed for CTC imaging using confocal laser endomicroscopy 6 weeks after the injection. Sections of blood vessels (0.453 $mm^2$) from each mouse were imaged for 20 min. (D) Mice orthotopically injected with vehicle (PBS, n = 2), SNU449$T_7$-shScram cells (n = 7), or SNU449$T_7$-shCD44 cells (n = 7) for 6 weeks were processed for collection of blood samples and the analysis of survival, and then the blood samples were processed and visualized using a fluorescent microscope after DAPI staining. The data represent three independent experiments.
191x192mm (300 x 300 DPI)

Figure 7-continued (LEE)

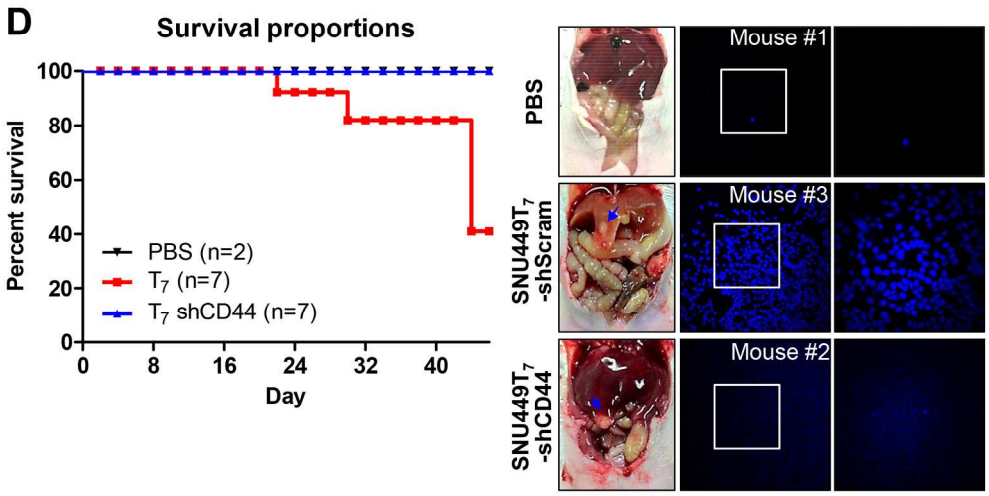


Fig. 7. Identification of TM4SF5-dependent CTCs and their metastasis. SNU449$T_7$ cells stably transfected with tGFP-shScram or tGFP-shTM4SF5 were orthotopically injected into livers (500,000 cells/mouse for 4 weeks or 200,000 cells/mouse for 6 weeks); separate injections of PBS alone were also performed as controls. (A) Four weeks later, blood samples collected from each mouse (middle images) were processed for FACS sorting (left histograms) and then seeded onto fibronectin-coated (10 μg/ml) coverslips prior to visualizing for tGFP (green) and staining with anti-tGFP antibody (red) or DAPI (blue). (B) The numbers of CTC-like cells sorted from the blood samples of mice injected with PBS (n = 5) were graphed at the mean ± SD, using SNU449$T_7$-tGFP-shScram cells (n = 10) or SNU449$T_7$-tGFP-shTM4SF5 cells (n = 5). (C) Mice orthotopically injected with SNU449$T_7$-tGFP-shScram (n = 3) or SNU449$T_7$-tGFP-shTM4SF5 (n = 3) were processed for CTC imaging using confocal laser endomicroscopy 6 weeks after the injection. Sections of blood vessels (0.453 $mm^2$) from each mouse were imaged for 20 min. (D) Mice orthotopically injected with vehicle (PBS, n = 2), SNU449$T_7$-shScram cells (n = 7), or SNU449$T_7$-shCD44 cells (n = 7) for 6 weeks were processed for collection of blood samples and the analysis of survival, and then the blood samples were processed and visualized using a fluorescent microscope after DAPI staining. The data represent three independent experiments.
186x103mm (300 x 300 DPI)

Figure 8 (LEE)

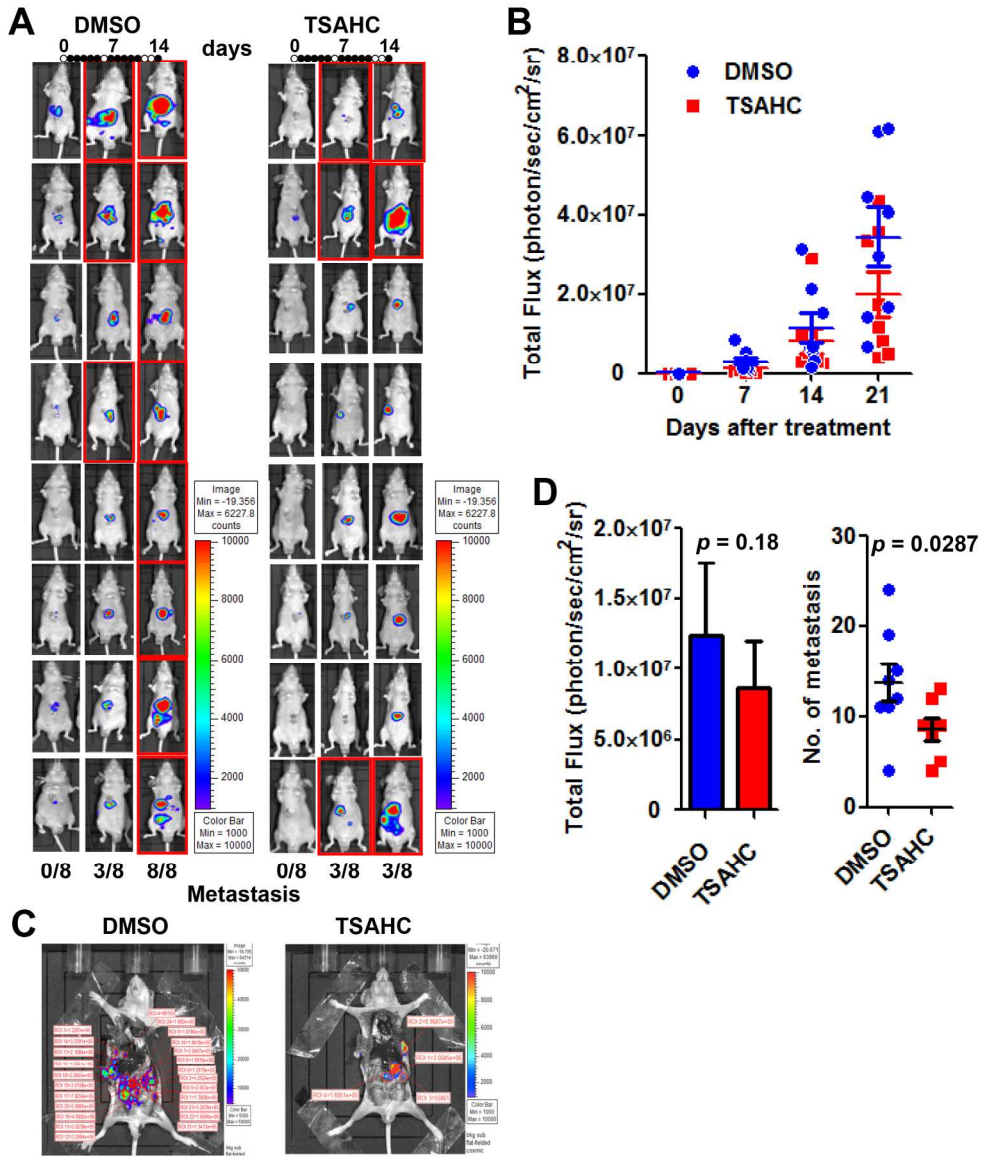


Fig. 8. Anti-TM4SF5 reagent blocked metastasis of orthotopically liver-injected cells to intestines. (A–E) Mice orthotopically liver-injected with SNU449T$_7$-pMSCV-Luc2 cells were treated with either DMSO or TSAHC, as explained in the Experimental Procedures. (A) Upto 2 weeks after the cell injection and treatment, bioluminescence images were saved. Mice marked with red rectangles depict mice with metastasized tumors. (B) The total bioluminescence flux after 3 week treatment were measured and shown as the mean ± SD. (C) Representative images of tumors in mouse treated with DMSO or TSAHC for 3 weeks. (D) Total flux (left) or number of metastatic tumors (right) was measured, and presented as the mean ± SD. $p \geq 0.05$ or $p < 0.05$ depicts statistical insignificance or significance, respectively. (E) Orthotopic tumors or metastatic tumors at the intestine or peritoneal membrane (Mem) were counted after abdominal surgery from each mouse treated with DMSO (n = 8) or TSAHC (n = 8) and graphed as the mean ± SD. The data represent three independent experiments. (F) Schematic model for TM4SF5-induced self-renewal capacity leading to CTC and liver-to-intestine metastases.
188x227mm (300 x 300 DPI)

Figure 8-continued (LEE)

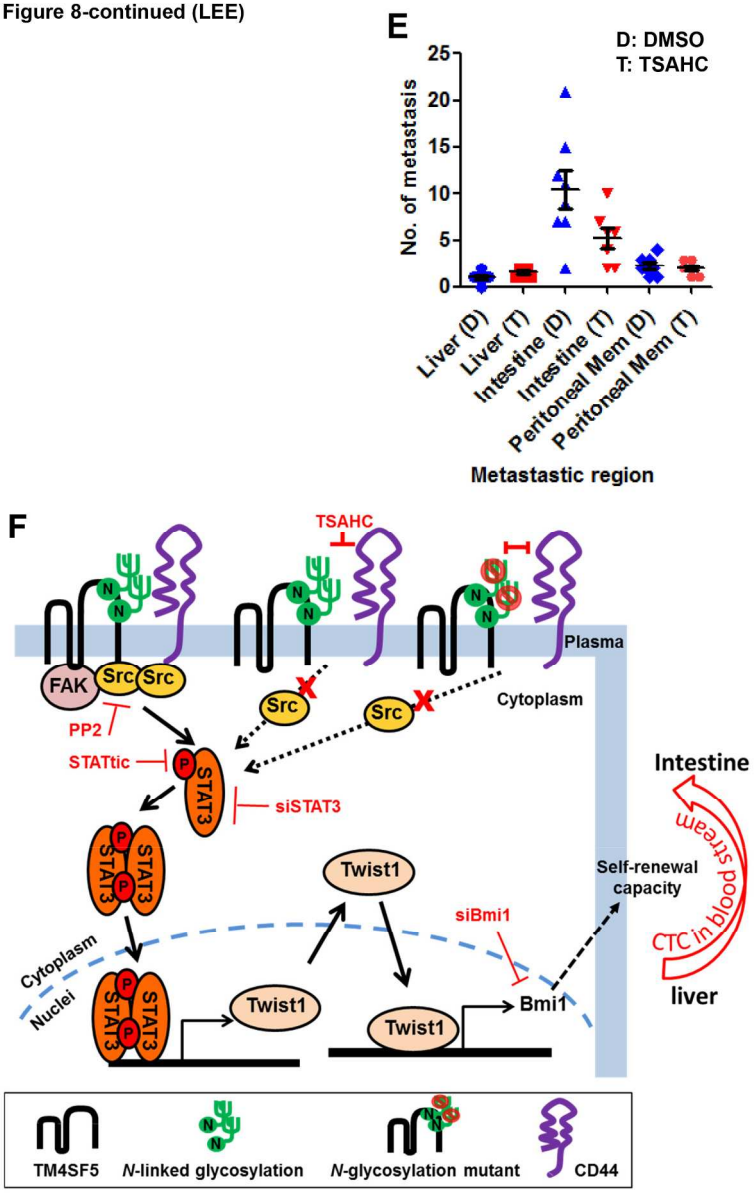


Fig. 8. Anti-TM4SF5 reagent blocked metastasis of orthotopically liver-injected cells to intestines. (A–E) Mice orthotopically liver-injected with SNU449T$_7$-pMSCV-Luc2 cells were treated with either DMSO or TSAHC, as explained in the Experimental Procedures. (A) Upto 2 weeks after the cell injection and treatment, bioluminescence images were saved. Mice marked with red rectangles depict mice with metastasized tumors. (B) The total bioluminescence flux after 3 week treatment were measured and shown as the mean ± SD. (C) Representative images of tumors in mouse treated with DMSO or TSAHC for 3 weeks. (D) Total flux (left) or number of metastatic tumors (right) was measured, and presented as the mean ± SD. $p \geq 0.05$ or $p < 0.05$ depicts statistical insignificance or significance, respectively. (E) Orthotopic tumors or metastatic tumors at the intestine or peritoneal membrane (Mem) were counted after abdominal surgery from each mouse treated with DMSO (n = 8) or TSAHC (n = 8) and graphed as the mean ± SD. The data represent three independent experiments. (F) Schematic model for TM4SF5-induced self-renewal capacity leading to CTC and liver-to-intestine metastases.
160x249mm (300 x 300 DPI)

**Interaction of tetraspan(in) TM4SF5 with CD44 promotes self-renewal and circulating capacities of hepatocarcinoma cells**

Doohyung Lee[1], Juri Na[2,*], Jihye Ryu[1,*], Hye-Jin Kim[1,*], Seo Hee Nam[3,*], Minkyung Kang[1,4], Jae Woo Jung[3], Mi-Sook Lee[1], Haeng Eun Song[1], Jungeun Choi[3], Gyu-Ho Lee[1], Tai Young Kim[1], June-Key Chung[2,5], Ki Hun Park[6], Sung-Hak Kim[7], Hyunggee Kim[7], Howon Seo[8], Pilhan Kim[8], Hyewon Youn[2,5], and Jung Weon Lee[1, 3,9]. *; equally contributed.

**This supplemental information includes supplemental Experimental procedures, References, and Figures.**

## EXPERIMENTAL PROCEDURES

***Cell Cultures.*** HCC cells, including SNU449 cells expressing WT TM4SF5 (SNU449Tp pooled clone, T3, T7, T10, and T16 single cell-derived clones), *N*-glycosylation mutants of TM4SF5 [N138A, N155Q, or N138A/N155Q (NANQ)], or no TM4SF5 [SNU449 parental (P) or Cp negative pooled clone], were previously described (1). Huh7 cells endogenously or SNU449$T_7$ clone exogenously expressing TM4SF5 were stably transfected with a scrambled control shRNA (tGFP-shScram in pGFP-V-RS plasmid, OriGene) or shRNA against TM4SF5 (2) [tGFP-shTM4SF5 in pGFP-V-RS plasmid, Cat. #: TG308787, OriGene). SNU449 and SNU761 cells do not express detectable levels of TM4SF5, whereas Huh7 and HepG2 cells express TM4SF5 (3). SNU449$T_7$ cells were also stably transfected with shRNA against CD44 (Addgene). Cells were maintained in RPMI-1640 medium (WelGene, Daegu, Korea) containing 10% FBS and 1% penicillin/streptomycin (GenDEPOT Inc.). Huh7 cells were sorted based on CD133 expression, and Huh7-CD133$^-$ cells were then stably transfected with TM4SF5. G418 (250 μg/ml, AG

Scientifics) or puromycin (7 μg/ml for Huh7 clones or 4 μg/ml for SNU449$T_7$ clones) were included in the culture media for stable cell clones and explant cells (isolated from the SNU449$T_7$-xenograft tumors).

***Drug sensitivity.*** Stable SNU449Cp (not expressing TM4SF5) or SNU449$T_7$ (TM4SF5-expressing) cells were seeded in 96-well plates (2000 cells/well). After 24 h, DMSO or paclitaxel (LC Laboratories) was added at different concentrations (0 to 100 nM), and the cells were cultured for an additional 48 h. Standard reading of MTT (Sigma) metabolites was performed at $OD_{540}$ and the mean ± standard deviation values were graphed.

***Spheroid formation assay.*** Cells were collected, washed twice with PBS to remove serum, and then suspended in serum-free DMEM/F12 media supplemented with 1% penicillin/streptomycin (GenDEPOT Inc.) and 2% B27 supplement (Invitrogen). Human EGF and bFGF (PeproTech, 25 ng/ml) were added to the culture every other day. The cells were subsequently cultured in ultra-low attachment 6-well plates (Corning Inc.) at a density of no more than $5 \times 10^3$ cells/well with or without specific inhibitors against TM4SF5 [TSAHC (4) 20 μM], c-Src (PP2 20 μM, LC Labs), or STAT3 (STATtics, 1 ~ 4 μM). The representative spheroid images were saved using a microscope (CKX41, Olympus, Tokyo, Japan) or a time-lapse IX81-ZDC microscope (Olympus).

***RT-PCR.*** Total RNA was isolated using TRIzol Reagent (Invitrogen), and complementary DNA (cDNA) was synthesized using an amfiRivert Platinum cDNA synthesis master mix (GenDEPOT) according to the manufacturer's instructions. The cDNA was subject to RT-PCR using the Dream Taq Green PCR master mix (Thermo Scientific) and primers, *β-actin* forward : 5'-TGACGGGGTCACCCACACTGTGCCCATCTA-3' and reverse : 5'-CTAGAAGCATTTGCGGTGGACGACGGAGGG-3', *CDH1 (E-Cadherin)*, forward 5'-

TGCCCAGAAAATGAAAAAGG-3' and reverse 5'-GTGTATGTGGCAATGCGTTC-3', *TM4SF5* forward : 5'-CTGCCTCGTCTGCATTGTGG-3' and reverse : 5'-CAGAAGACACCACTGGTCGCG-3', *CD24* forward : 5'-AACTAATGCCACCACCAAGG-3' and reverse : 5'-CCTGTTTTTCCTTGCCACAT-3', *CD44* forward : 5'-CGGACACCATGGACAAGTTT-3' and reverse : GAAAGCCTTGCAGAGGTCAG-3', *Twist1* forward : 5'-GGAGTCCGCAGTCTTACGAG-3' and reverse : 5'-TCTGGAGGACCTGGTAGAGG-3', *Bmi1* forward : 5'-GAGAAATCTAAGGAGGAGGTGAA-3' and reverse : 5'-TGG AAATGTGAGGAAACTGTGG-3'.

***Western blots.*** Subconfluent cells in media containing 10% FBS, or spheroids were harvested for whole cell lysates using a modified RIPA lysis buffer containing 0.1% SDS, 0.5% deoxycholate, 1% NP-40, and proteinase inhibitors (1). Tissue extracts from human or mouse livers were also prepared as previously described (1). The primary antibodies included CD44 (clone IM7 from BioLegend, clone DF1485 from Santa Cruz Biotech.), CD133 (Miltenyi), STAT3 (Chemicon), phospho-$Y^{705}$STAT3 (Millipore), Bmi1, phospho-$Y^{397}$FAK (Abcam, Cambridge, UK), phospho-$Y^{416}$c-Src (Cell Signaling Technol.), phospho-$Y^{577}$FAK, p$S^{10}$p$27^{Kip1}$, c-Src, phospho-$S^{727}$STAT3 (Santa Cruz Biotech.), FAK, $p27^{Kip1}$ (BD Transduct. Lab.), ZO-1 (Zymed Lab), α-tubulin (Sigma), and anti-TM4SF5(1).

***Coimmunoprecipitations.*** Whole cell extracts obtained 48 h after transient transfection of cells with Strep-tagged mock, strep-tagged WT TM4SF5, strep-tagged TM4SF5 N138AN155Q mutant, WT CD44, and/or mutant CD44 were incubated with precoated biotin beads (IBA, Hanover, Germany) for 2 h. For treatment experiments, the transfected cells were treated with DMSO vehicle or 20 μM TSAHC (4) for another 24 h prior to whole cell lysate preparation.

Immunoprecipitated proteins were boiled in 2× SDS-PAGE sample buffer before standard western blotting.

***ALDERFLUOR assay.*** Aldehyde dehydrogenase **(**ALDH) activity was measured in the SNU449 stable cells using the ALDEFLUOR assay kit (StemCell Technologies) according to the manufacturer's protocol. Briefly, the cells were harvested, placed in ALDEFLUOR® assay buffer ($6 \times 10^5$ cells/ml), and incubated with the ALDEFLUOR® substrate for 45 min at 37°C. As a negative control, an aliquot of ALDEFLUOR®-stained cells was immediately quenched with diethylaminobenzaldehyde, a specific ALDH inhibitor. The cells were analyzed using a FACS Calibur flow cytometer (BD Biosciences).

***Flow cytometry.*** Stable SNU449 cell clones with or without TSAHC treatment, cells prepared from primary or secondary xenograft tumors, and cells sorted from blood samples were processed for FACS analysis, as previously described (5). The primary antibodies used included antibodies against CD24, CD44 (clone DF1485 or clone IM7), CD90, CD133 (BioLegend), and TM4SF5 (6) (Clone # 27). Double staining for TM4SF5 (clone #27) and CD44 (clone DF1485) was also performed. Controls without primary or secondary antibodies were also performed in parallel.

***Serial mouse xenografts.*** Three- or four-weeks old male BALB/c-nu/nu mice were purchased from Orient Co. Ltd (Seungnam, Korea). The mice were housed in a specific pathogen-free room under controlled temperature and humidity. All animal procedures were performed in accordance with the procedures in the Seoul National University Laboratory Animal Maintenance Manual and with Institutional Review Board approval. Viable SNU449Cp, $SNU449_{N138A/N155Q}$ (NANQ), or $SNU449T_7$ cells suspended in Matrigel (BD Biosciences) premixed with RPMI-1640 medium and 10% FBS were injected subcutaneously at the indicated cell numbers into the left or right

flank of mice. Tumor formation was monitored weekly for 6 weeks and tumor volumes were measured as described previously (1). For serial xenograft injection, tumors were minced into approximately 1 $mm^3$ pieces and incubated with type II collagenase (Gibco) and DNase I (Takara Bio Inc.) for 0.5 to 1 h at 37ºC under constant rotation (60 rpm). A single-cell suspension was obtained by filtering the supernatant through a 40-μm cell strainer (BD Biosciences), and explant cells were maintained with culture medium containing G418 (250 μg/ml, A.G. scientific Inc.) to select for TM4SF5 expressing cells.

***Immunohistochemistry of mouse or human tissues*.** All procedures in animal and human tissues were performed in accordance with the procedures of the Seoul National University Institutional Review Board (SNUIRB) agreement. Dissected 6-μm-thick slices of human liver tissues were obtained with informed content from patients who received surgery at the National Biobank of Korea-Pusan National University Hospital (PNUH) in accordance with IRB agreements. The tissues were processed, paraffin embedded, and sectioned. After deparaffinization, antigen retrieval was performed by boiling the sections for 5 min in sodium citrate solution (0.01 M, pH 6.0). The sections were incubated at 4ºC with the indicated antibodies in PBST (0.3% Triton X-100 in PBS) containing 5% goat serum or 3% BSA. After washing, the sections were incubated with biotin-conjugated anti-rabbit, -mouse or -goat IgG (1:100, Sigma) antibody and ExtrAvidin-peroxidase (1:50, Sigma) at room temperature for 1 h each for 3,3′-diaminobenzidine detection. The sections were counterstained with hematoxylin and imaged under a microscope. Immunohistochemistry analysis of serial sections from the same tumor regions or xenografts was performed using normal rabbit IgG, normal mouse IgG, anti-TM4SF5 (Clone # 27), anti-CD44 (clone IM7), and anti-Bmi1 (Abcam) antibodies. Double-immunostaining of mouse xenograft tissues was processed for immunohistochemistry using primary antibodies as described above

and imaged using a fluorescence microscope (BX51TR, Tokyo, Olympus).

***Orthotopic tumor cell injection and blood collection for CTC identification.*** Male BALB/c nude mice (5 or 6 weeks old) were used for these experiments. SNU449$T_7$ cells were stably transfected with pGFP-V-RS shScramble or shTM4SF5 (Origene Technologies, Inc.), and selected by puromycin treatment (4 μg/ml, Sigma). To generate orthotopic liver tumor model, 5 × $10^5$ cells stably transfected with SNU449$T_7$-shScramble or -shTM4SF5 were resuspended in PBS (50 μl) and injected into the left lobes of mouse livers. To identify CTCs, blood samples were collected by cardiac puncture at 4 or 6 weeks after cell injection. Peripheral blood mononucleated cells (PMBCs) were purified from the blood samples using a density gradient. GFP-positive PMBCs were sorted using a FACSAria III cell sorter (BD Bioscience). The isolated GFP-positive cells were seeded onto fibronectin-coated (10 μg/ml) cover slips and tGFP (Origene Technologies, Inc.), anti-tGFP, and DAPI immunofluorescence was imaged using a fluorescent microscope (BX51TR, Tokyo, Olympus).

***Metastatic evaluation of orthotopically liver-implanted cells.*** SNU449$T_7$ cells were stably transfected with pMSCV-Luc2. After minimal incision, 1 x $10^5$ cells of luciferase-expressing SNU449$T_7$ were orthotopically implanted in the liver of BALB/c nude mouse (6 weeks old male). DMSO or TSHAC (20 mg/kg body weight) was treated by i.p. injection for 5 days in a week, and bioluminescence from SNU449$T_7$ cells were acquired in an IVIS Luminar imaging system (Perkin Elmer, Santa Clara, CA). Mice were kept on the imaging stage under anesthesia with 1.5% isoflurane gas at a flow rate of 1.5L/min. Before image acquisition, 150 mg/kg body weight of D-luciferin (Molecular Probes, Invitrogen, Carlsbad, CA) was administrated by i.p. injection and bioluminescence signals were collected at 10-30 min with maximum intensity. The signals of emitted from cells were presented as pseudo-color spectra ranging from red

(maximum) to blue (minimum) based on their intensity. Gray-scale photographs of mouse and corresponding pseudo-color images were superimposed with LIVINGIMAGE version 2.12 (Xenogen, Alameda, CA) and IGOR version 1.24 (WaveMetrics, Portland, OR) image analysis software. Signals emitted by regions of interest (ROI) were measured and expressed as photon flux [photons/sec/$cm^2$/steradian], which refers to the photons emitted from a unit solid angle of a sphere. The background signal intensity was subtracted electronically for normalization both from images and from the measurements of photon flux. Number of metastasis was counted by number of ROIs.

**References**


1. Lee SA, Lee SY, Cho IH, et al. Tetraspanin TM4SF5 mediates loss of contact inhibition through epithelial-mesenchymal transition in human hepatocarcinoma. *J Clin Invest*. 2008;118:1354-1366.
2. Jung O, Choi YJ, Kwak TK, et al. The COOH-terminus of TM4SF5 in hepatoma cell lines regulates c-Src to form invasive protrusions via EGFR Tyr845 phosphorylation. *Biochim Biophys Acta*. 2013;1833:629-642.
3. Choi S, Oh SR, Lee SA, et al. Regulation of TM4SF5-mediated tumorigenesis through induction of cell detachment and death by tiarellic acid. *Biochim Biophys Acta*. 2008;1783:1632-1641.
4. Lee SA, Ryu HW, Kim YM, et al. Blockade of four-transmembrane L6 family member 5 (TM4SF5)-mediated tumorigenicity in hepatocytes by a synthetic chalcone derivative. *Hepatology*. 2009;49:1316-1325.
5. Kim H-P, Kim T-Y, Lee M-S, et al. TGF-[beta]1-mediated activations of c-Src and Rac1 modulate levels of cyclins and p27Kip1 CDK inhibitor in hepatoma cells replated on fibronectin. *Biochimica et Biophysica Acta (BBA) - Molecular Cell Research*. 2005;1743:151-161.
6. Kang M, Ryu J, Lee D, et al. Correlations between Transmembrane 4 L6 family member 5 (TM4SF5), CD151, and CD63 in liver fibrotic phenotypes and hepatic migration and invasive capacities. *PLoS ONE*. 2014;9:e102817.

**Supplementary figures**

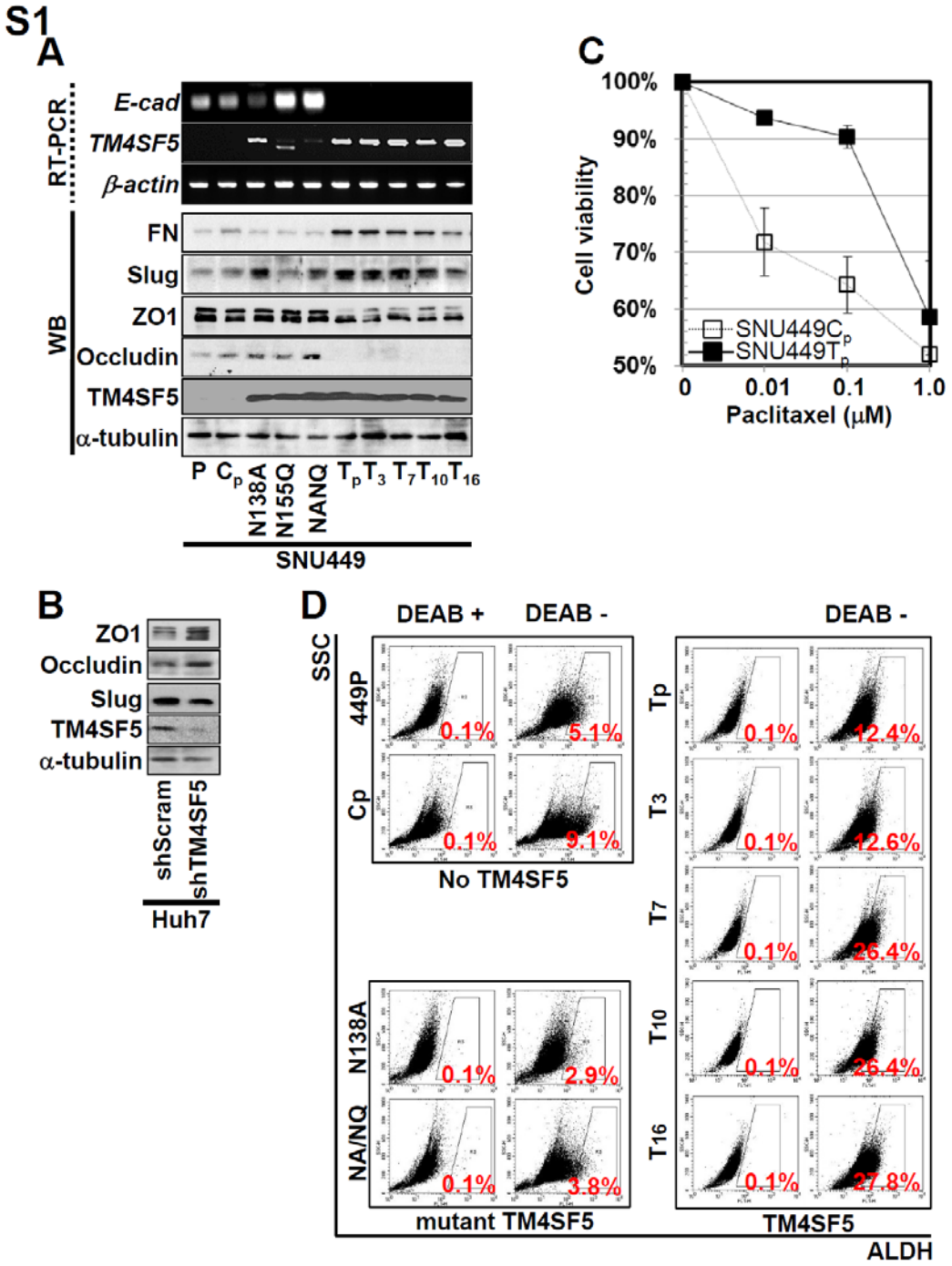


**Figure S1. TM4SF5-mediated ECM phenotypes and enhanced aldehyde dehydrogenase (ALDH) positivity. (A)** Subconfluent stable SNU449 hepatocarcinoma cell clones (P; parental lacking for TM4SF5 expression, Cp; negative control, NANQ; mutant of the *N*-glycosylation residues of N138 and N115, $T_p$; TM4SF5-positive pooled clone, $T_3$ ~ $T_{16}$; TM4SF5-positive single cell-derived clones) were processed for standard Western blots or RT-PCR. **(B)** Huh7 cells

were stably transfected with shRNA against a scramble sequence (shScram) or a sequence in TM4SF5 (shTM4SF5). Whole cell lysates were processed for the standard Western blots against the indicated molecules. **(C)** TM4SF5-negative SNU449Cp and TM4SF5-positive SNU449Tp cells were treated with either vehicle (0 μM) or different concentrations of paclitaxel (0.01, 0.1, or 1.0 μM) for 24 h, prior to MTT assay to analyze cell viability. Each value was in triplicate and shown at mean ± standard deviation (SD). **(D)** The stable SNU449 clones were processed for ALDH activity assay, using a specific inhibitor of ALDH, diethylaminobenzaldehyde (DEAB) for background fluorescence. The values in % indicate the population of ALDH-positive cells at each experimental condition. Data shown represent three independent experiments.

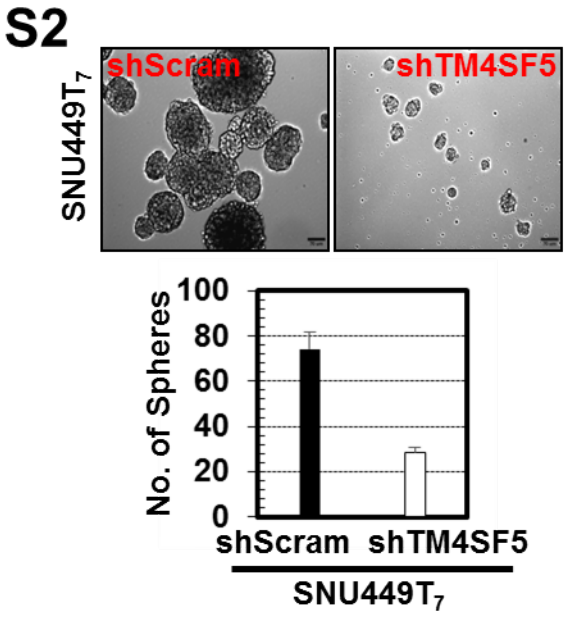


**Figure S2. Suppression of TM4SF5 in SNU449T$_7$ cells resulted in a less formation of spheres.** G418-resistant and TM4SF5-expressing SNU449T$_7$ cell clones were stably transfected with GFP-shRNA (a scramble sequence, shScram) or GFP-shTM4SF5 via puromycin selection. The cells were analyzed for sphere formation in a less adhesive condition for 10 days and then the numbers of spheres were counted under a microscope. The values at mean ± SD were presented in the graph.

S3

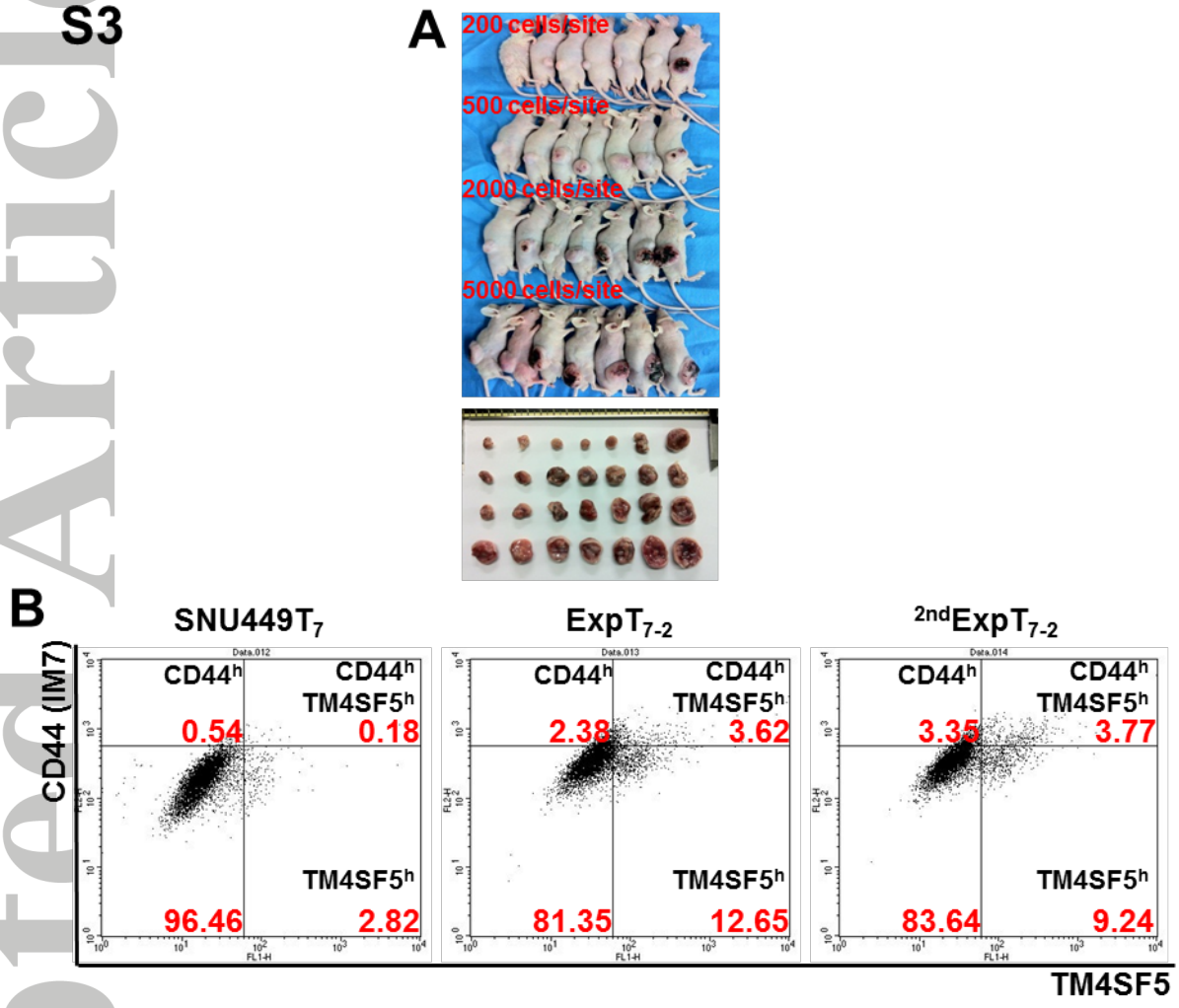


**Figure S3. The serial xenografts of TM4SF5-expressing SNU449T$_7$ cell clones at small numbers of the cells. (A)** Viable ExpT$_{7-2}$ cells (cells purified from the primary xenograft after injection of SNU449T$_7$ cells to mouse #2) suspended in Matrigel (BD Biosciences) premixed with RPMI-1640 medium and 10% FBS at the indicated cell numbers were injected subcutaneously in the flanks of mice. Four weeks later, the images were saved. **(B)** The cells purified from xenografts (ExpT$_{7-2}$ from the primary xenograft with SNU449T$_7$; $^{2nd}$ExpT$_{7-2}$ from the second xenograft injected with ExpT$_{7-2}$) and SNU449T$_7$ cells were analyzed for CD44 (anti-CD44 antibody IM7 clone) and TM4SF5 using flow cytometry. The numbers in red indicate the percentage of populations of cells showing enhanced CD44 (CD44$^h$), TM4SF5 (TM4SF5$^h$) alone or both (CD44$^h$/TM4SF5$^h$) after each xenograft, compared their levels in SNU449T$_7$. Data shown present there independent experiments.

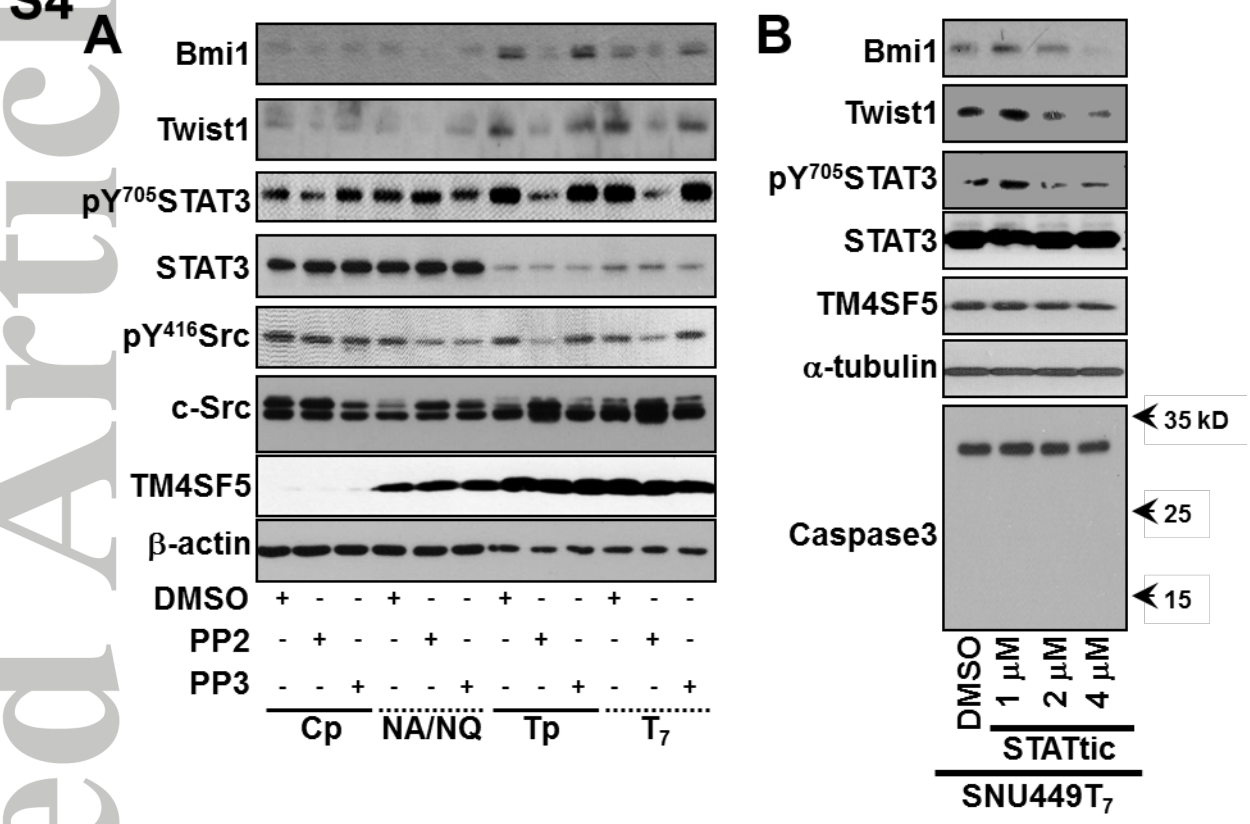


**Figure S4. TM4SF5-mediated signaling activities after c-Src or STAT3 inhibitions.** The stable SNU449 cell clones (Cp; TM4SF5-negative control pooled SNU449 clone, NANQ; SNU449 clone to express N138A/N155Q *N*-glycosylation mutant, Tp or $T_7$; TM4SF5-expressing pooled or single cell-derived SNU449 clone, respectively) were treated with either DMSO (vehicle), PP2 (a specific c-Src inhibitor, 20 μM), PP3 (a negative control compound, 20 μM) **(A)**, or STATtic (STAT3 inhibitor, 1 to 4 μM) **(B)** for 24 h, prior to whole cell lysate harvest and standard Western blots. Data shown represent three different experiments.

**S5**

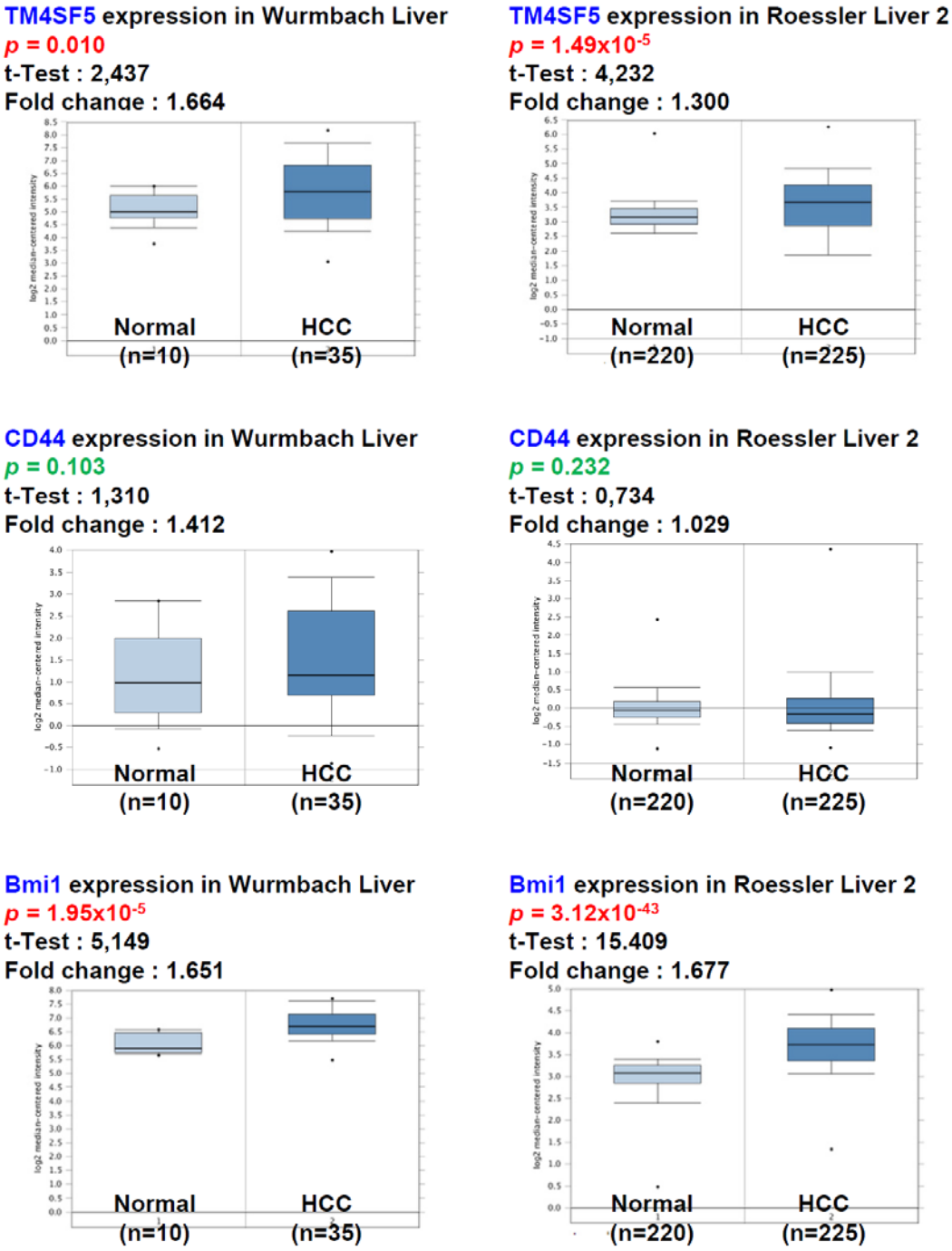


**Figure S5. Positive correlations between TM4SF5 and Bmi1 expression levels enhanced in hepatocellular carcinoma, compared with those in normal counterparts.** The data were retrieved from an online database (i.e., Oncomine, www.oncomine.org).

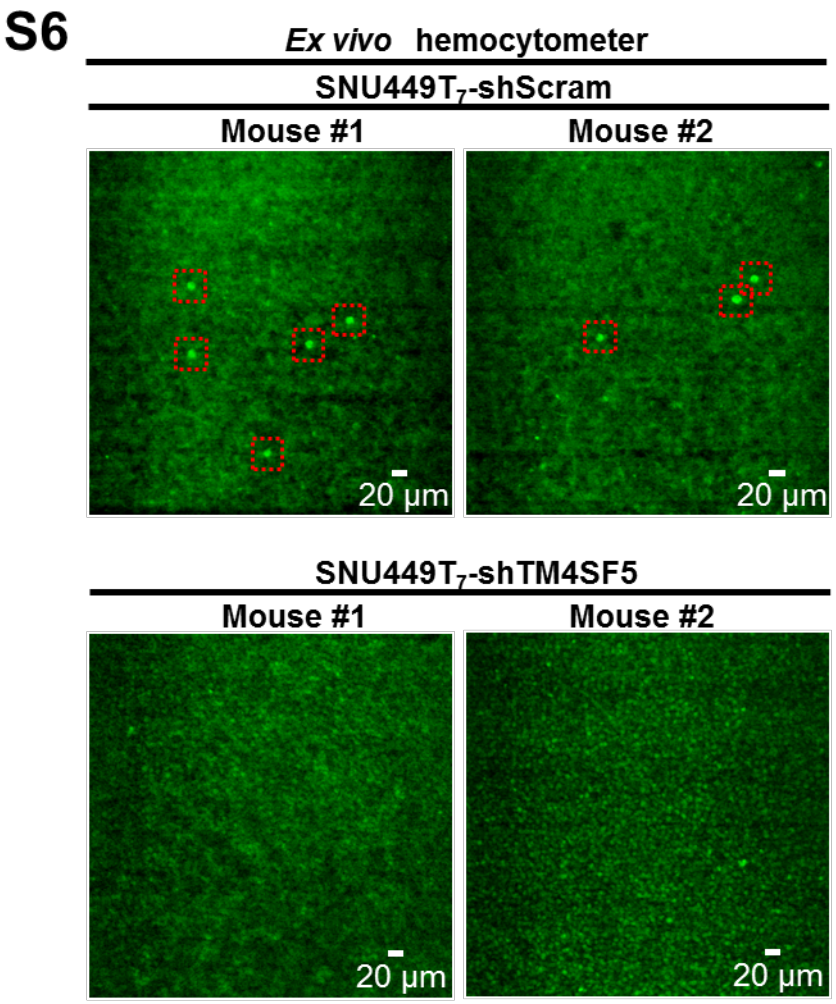


**Figure S6. Existence of TM4SF5-positive cells in the blood samples of mice orthotopically liver-injected with SNU449T$_7$ cells stably transfected with either GFP-shScram (against a control scrambled sequence) or GFP-shTM4SF5.** The cells (5 x $10^5$ cells/mouse) were orthotopically injected into livers and 6 weeks later the mice (n =3) were sacrificed to collect the blood samples, prior to visualization of the TM4SF5-positive green cells.